New Journal of Physics
The open access journal at the forefront of physics

PAPER • OPEN ACCESS

Jerky chiral active particles

To cite this article: Stephy Jose and Hartmut Löwen 2025 *New J. Phys.* **27** 115003

IOP Publishing New J. Phys. 27 (2025) 115003 https://doi.org/10.1088/1367-2630/ae1c65

New Journal of Physics
The open access journal at the forefront of physics

Deutsche Physikalische Gesellschaft DPG
IOP Institute of Physics

Published in partnership with: Deutsche Physikalische Gesellschaft and the Institute of Physics

PAPER

Jerky chiral active particles

Stephy Jose* and Hartmut Löwen

Institut für Theoretische Physik II: Weiche Materie, Heinrich-Heine-Universität Düsseldorf, D-40225 Düsseldorf, Germany
* Author to whom any correspondence should be addressed.

E-mail: stephy.jose@hhu.de and hlowen@thphy.uni-duesseldorf.de

Keywords: jerk, chirality, active matter, active Brownian particle, circle swimmers

OPEN ACCESS

RECEIVED
26 August 2025

REVISED
25 October 2025

ACCEPTED FOR PUBLICATION
6 November 2025

PUBLISHED
26 November 2025

Abstract

We introduce jerky chiral active Brownian particles (ABP), a generalization of conventional chiral ABPs subjected to jerk, the time derivative of acceleration, and analytically derive their mean displacement and mean squared displacement. Our results show that jerk induces anomalous fluctuations and oscillatory behavior on the standard circular swimming of chiral active particles. The interplay of jerk, chirality and persistence produces a family of mean trajectories including damped and exploding Lissajous patterns alongside the well-known *spira mirabilis* (logarithmic spirals). Our work on jerky chiral active particles opens a new route to explore rich dynamical effects in active matter.

The time derivative of acceleration, known as *jerk*, quantifies how rapidly acceleration changes with time. Although the origin of the term 'jerk' itself is uncertain, early references to the rate of change of acceleration can be found in the works of Transon (1845), who described a related concept termed *virtualité* [1], and Meyer (1959), who later used the German term *Ruck* to denote the same physical quantity [2]. Schot provided a systematic treatment of jerk in modern mechanics, focusing on its geometric and physical interpretation in planar motion [3]. He emphasized the role of jerk in ensuring smooth transitions, particularly in engineering design, vehicle dynamics, and human comfort. In mechanical systems, large or discontinuous jerk leads to sudden force changes, vibration, and contact loss, producing higher peak loads, wear, and noise. Controlling jerk therefore keeps forces smooth, reduces mechanical fatigue, and enables quieter and longer-lived machines. For instance, cam design is essentially an exercise in jerk optimization. Similarly, in transportation, easement (transition) curves are used to connect straight and curved paths gradually. These curves minimize abrupt curvature changes, thereby reducing jerk and improving passenger comfort.

Linz later showed that even simple nonlinear systems can give rise to complex jerk dynamics, and that several canonical chaotic models can be reformulated in the form of jerk equations, providing a compact representation of their underlying motion [4]. Building on this, Eichhorn *et al* classified broad families of such systems and demonstrated that even minimal jerk formulations can generate deterministic chaos [5, 6]. The notion of jerk is also relevant in understanding biological motion. Many organisms from migrating cells and swimming microorganisms to flying insects and foraging sea turtles exhibit complex trajectories shaped by higher-order temporal correlations in their movement dynamics [7]. In addition, the concept of jerk is used in traffic flow control [8], in the Abraham–Lorentz force describing radiation reaction [9], and even in cosmology, where cosmic jerk parameters quantify the rate of change of cosmic acceleration [10].

Memory effects can also give rise to effective jerk dependence. In many physical systems, memory arise from coarse-graining over hidden degrees of freedom, delayed feedback, history-dependent friction, or time-correlated noise [11–30]. One minimal way to model such memory is to include jerk, in the equations of motion [3–6, 31–36]. In colloidal systems immersed in viscoelastic or non-Newtonian fluids, the frictional force is not instantaneous but instead depends on the entire history of particle through a memory kernel [37–42]. Expanding such memory kernels leads to terms proportional to jerk [43]. Advances in engineering have enabled the experimental realization of feedback-controlled systems using synthetic forces leading to effective dynamics with time delays [44–48]. When an external force is applied

based on delayed measurements of the motion of a particle, the resulting dynamics can involve an explicit dependence on the acceleration of the particle and its rate of change [43]. Such systems challenge the foundational assumptions of classical mechanics, such as the force depending only on the velocity or the positivity of the inertial mass [49]. They describe physically realizable systems with rich and often counterintuitive dynamics.

Far from equilibrium, memory becomes even more prominent [50, 51]. The presence of memory fundamentally alters transport, fluctuations, and response in stochastic systems [52, 53]. It can induce anomalous diffusion, modify relaxation spectra, and lead to long-range temporal correlations [54–58]. A paradigmatic example is active matter [59–62] composed of self-driven entities that consume energy to generate motion. Examples of active matter span a wide range of scales and materials from natural systems such as motile bacteria and eukaryotic cells [63, 64], to artificial systems such as synthetic colloidal swimmers [65–67] and active granular rods [68, 69]. A central goal in active matter physics is to understand how simple rules of individual propulsion and interaction give rise to complex collective dynamics and non-equilibrium phases. A widely studied model is the active Ornstein–Uhlenbeck process, where self-propulsion arises from temporally correlated (colored) noise, endowing the particle with a finite persistence time, a form of memory in its motion [70–78]. Another simple microscopic model of active matter is the overdamped active Brownian particle (ABP), in which a particle moves with a fixed propulsion speed along a fixed direction that undergoes rotational diffusion [79–83]. Despite its simplicity, these models capture a wide range of interesting phenomena such as enhanced diffusion, ballistic-diffusive crossover, boundary accumulation, and motility induced phase separation [61, 84–87].

More recently, significant attention has turned to models incorporating *inertia* and underdamped ABPs have been proposed to describe active particles in dilute gases, vacuum, or low-viscosity fluids [88–98]. They have a mass and characterize dynamics over both the inertial timescale and the rotational persistence timescale. Inertia leads to persistent velocity correlations [99, 100], transient superdiffusion [93, 96], and effective temperatures [101, 102]. In parallel, active matter models with *chirality* have been introduced to capture the effects of broken rotational symmetry on the dynamics of self-propelled particles [62, 69, 93, 103–108]. These models typically prescribe a constant angular velocity to the orientation dynamics, resulting in circular trajectories in the absence of rotational noise [103, 109, 110]. The noise-averaged mean displacement follows a *spira mirabilis* or logarithmic spiral [93, 103]. Chiral active particles display a range of interesting behaviors, including spiral drift, surface accumulation, circular confinement, and complex scattering dynamics [103, 111–113]. Beyond inertia and chirality, a new class of active particles incorporating jerk has recently been introduced [43, 114]. *Te Vrugt et al* [114] presents a field-theoretical approach with an additional intrinsic timescale, while [43] extends the active Ornstein–Uhlenbeck model to include jerk, revealing anomalously large fluctuations and super-ballistic mean-squared displacement (MSD).

In this work, we introduce a jerky chiral ABP (jcABP) model by incorporating jerk in the translational equation of motion and chirality via a constant angular velocity in the orientational equation of motion in two dimensions. This model enables us to systematically investigate the impact of jerk, inertia, and chirality in active particle dynamics. We analytically derive the Green's function, and exact expressions for mean displacement and MSD in various limiting cases. We demonstrate that jerk induces transient oscillations in both the mean trajectory and the MSD, even in the absence of chirality. When combined with chirality, jerk fundamentally alters the circular swimming behavior of active particles. Specifically, we find that the radius of the emergent orbit becomes a non-trivial function of the jerk time scale. In the presence of rotational noise, the interplay between jerk, chirality, and persistence leads to spiral trajectories resembling *Lissajous* curves. The shape of the trajectories crucially depend on the relative values of different underlying parameters. We also show that jerk introduces anomalous fluctuations characterized by unusually high power-law exponents at short times.

This paper is organized as follows. In section 1, we introduce the model. In section 2, we derive the orientation correlation functions and the Green's function. In section 3, we consider the limiting case of vanishing chirality and obtain exact expressions for the mean displacement and the MSD. Here we show that jerk induces oscillatory behavior in the cumulants of the displacement and anomalous short-time fluctuations characterized by a t^5 scaling. In section 4, we analyze the effects of finite chirality, treating separately the cases with and without rotational noise. Without rotational noise, the particle follows circular trajectories at long times, with a radius that depends non-trivially on chirality as well as the friction and jerk timescales. In the presence of rotational noise, we obtain spiral trajectories which resemble intricate Lissajous patterns with beats and modulations. Depending on the parameter values, these curves can be either damped or exploding. We present conclusions and discussion in section 5. Finally, details pertaining to a few calculations in the main text are provided in appendices A and B.

1. Model

We consider a two-dimensional ABP subject to jerk, inertia, and chirality, driven by both self-propulsion and thermal noise. The position of the particle $\vec{r}(t) = (x(t), y(t))$ evolves according to the third-order Langevin equation:

$$\lambda \dddot{\vec{r}}(t) + m\ddot{\vec{r}}(t) + \gamma\dot{\vec{r}}(t) = \gamma v_0 \hat{n}(t) + \sqrt{2D\gamma^2}\vec{\eta}(t), \tag{1}$$

$\vec{F}_{\text{act}}(t)$ $\vec{F}_{\text{therm}}(t)$ where λ is the coefficient of the jerk, m is the mass of the particle, and γ is the viscous friction coefficient. The above equation also appears in [43], where it is studied in one dimension for an active Ornstein–Uhlenbeck particle in the absence of thermal noise. The right-hand side of equation (1) includes a self-propulsion force of magnitude γv_0 along the instantaneous orientation $\hat{n}(t) = (\cos\theta(t), \sin\theta(t))$, as well as a stochastic thermal force modeled by a Gaussian white noise $\vec{\eta}(t)$ with vanishing mean $\langle \eta_i(t) \rangle = 0$ and delta correlations $\langle \eta_i(t')\eta_j(t'') \rangle = \delta_{ij}\delta(t' - t'')$. Also, v_0 is the constant self-propulsion velocity and D is the translational diffusion constant. Note that the same form of equation (1) also applies to a passive particle when the self-propulsion term is set to zero, corresponding to a jerky passive particle which is analyzed in detail in [43].

The orientation angle $\theta(t)$ evolves independently via angular velocity ω_0 (chirality) and a stochastic rotational diffusion term:

$$\dot{\theta}(t) = \omega_0 + \sqrt{2D_r}\eta_r(t), \tag{2}$$

where D_r is the rotational diffusion constant and $\eta_r(t)$ is a Gaussian white noise with vanishing mean $\langle \eta_r \rangle = 0$ and delta correlation $\langle \eta_r(t')\eta_r(t'') \rangle = \delta(t' - t'')$. The angular noise drives decorrelation of the orientation over a characteristic time scale $1/D_r$, while ω_0 introduces persistent circular motion and chirality. In this framework, the particle's position $\vec{r}(t)$ describes a stochastic trajectory in the x–y plane. The instantaneous magnitude of the position vector is given by $r(t) = |\vec{r}(t)| = \sqrt{x(t)^2 + y(t)^2}$, and the azimuthal angle in real space is $\phi(t) = \tan^{-1}(y(t)/x(t))$. Note that $\phi(t)$ is distinct from the internal propulsion angle $\theta(t)$, which governs the direction of self-propulsion. Figure 1 provides a schematic representation of a jerky chiral active particle.

We identify the relevant time scales in the system: the jerk time scale $\tau_J = \lambda/m$, the friction time scale $\tau_F = \sqrt{\lambda/\gamma}$, the persistence time scale of the rotational noise $\tau_P = 1/D_r$, and the chiral time scale $\tau_C = 1/\omega_0$. In terms of these quantities, equation (1) becomes

$$\dddot{\vec{r}}(t) + \ddot{\vec{r}}(t)/\tau_J + \dot{\vec{r}}(t)/{\tau_F}^2 = (\gamma v_0/\lambda)\,\hat{n}(t) + \sqrt{2D\gamma^2/\lambda^2}\,\vec{\eta}(t). \tag{3}$$

We take the persistence time τ_P as the natural time unit and the persistence length $l_P = v_0\tau_P$ as the natural length unit. For simplicity, we assume that the particle is completely at rest at time $t = 0$ and consider initial conditions of the form:

$$\vec{r}(0) = \dot{\vec{r}}(0) = \ddot{\vec{r}}(0) = \vec{0} \text{ and } \theta(0) = 0. \tag{4}$$

We next systematically analyze equation (3) to derive the Green's function, and cumulants of the displacement $\vec{r}(t)$.

2. Orientation correlations and Green's function

The orientation correlation function is given as [88, 93] (see appendix A for a derivation)

$$\langle \hat{n}(t') \cdot \hat{n}(t'') \rangle = \cos\left[(t' - t'')/\tau_C\right] \mathrm{e}^{-|t' - t''|/\tau_P}. \tag{5}$$

This correlation function captures both the exponential decay due to rotational diffusion and the oscillatory behavior due to chirality. As we will see, it enters as a kernel in the evaluation of the cumulants of the displacement. Let us define the Green's function $G(t)$ as the response to a δ-kick. Due to isotropy and linearity, the Green's function is diagonal and scalar-valued:

$$\lambda \dddot{G}(t) + m\ddot{G}(t) + \gamma\dot{G}(t) = \delta(t). \tag{6}$$

The Green's function describes the linear response of the translational motion and remains isotropic, since the coefficients λ, m, and γ are scalar. Chirality enters only through the orientation dynamics in

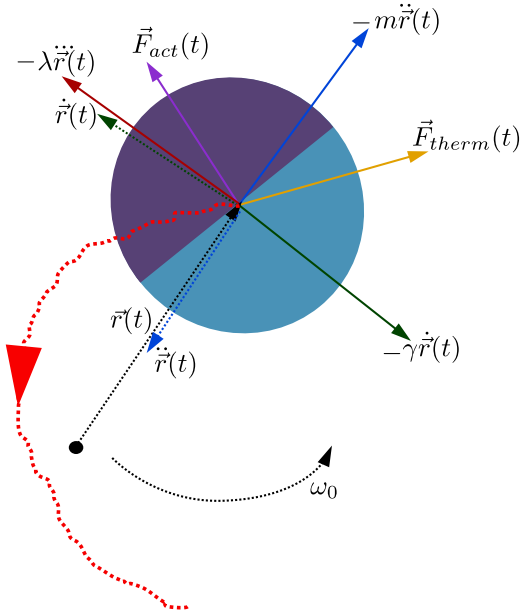

Figure 1. Schematic representation of a jerky chiral active particle. The particle's position $\vec{r}(t)$ evolves under the combined influence of five terms: the jerk term $-\lambda\dddot{\vec{r}}(t)$, the inertial term $-m\ddot{\vec{r}}(t)$, the viscous drag $-\gamma\dot{\vec{r}}(t)$, and the active and thermal forces $\vec{F}_{\rm act}(t)$ and $\vec{F}_{\rm therm}(t)$ respectively. The active force $\vec{F}_{\rm act}(t) = \gamma v_0 \hat{n}(t)$ acts along the instantaneous orientation $\hat{n}(t)$, which itself rotates at an angular velocity ω_0, introducing chirality into the motion. The stochastic thermal force $\vec{F}_{\rm therm}(t) = \sqrt{2D\gamma^2}\vec{\eta}(t)$ produces random thermal fluctuations.

equation (2). To proceed, we define the one-dimensional Fourier transform of a function $f(t)$ and its inverse $\tilde{f}(\omega)$ as

$$\tilde{f}(\omega) = \int_{-\infty}^{\infty} \mathrm{d}t\, \mathrm{e}^{\mathrm{i}\omega t} f(t)\,,$$
$$f(t) = \frac{1}{2\pi}\int_{-\infty}^{\infty} \mathrm{d}\omega\, \mathrm{e}^{-\mathrm{i}\omega t}\tilde{f}(\omega)\,. \tag{7}$$

Taking the Fourier transform of both sides of equation (6) yields

$$(i\omega)^3 \lambda\tilde{G}(\omega) + (\mathrm{i}\omega)^2 m\tilde{G}(\omega) + (\mathrm{i}\omega)\gamma\tilde{G}(\omega) = 1. \tag{8}$$

So the Green's function in Fourier space is

$$\tilde{G}(\omega) = \frac{1}{\mathrm{i}\lambda\omega^3 - m\omega^2 - \mathrm{i}\gamma\omega}. \tag{9}$$

The time-domain response is obtained by computing the inverse Fourier transform:

$$G(t) = \frac{1}{2\pi}\int_{-\infty}^{\infty} \frac{\mathrm{e}^{-\mathrm{i}\omega t}}{\mathrm{i}\lambda\omega^3 - m\omega^2 - \mathrm{i}\gamma\omega}\,\mathrm{d}\omega. \tag{10}$$

We evaluate this integral by contour integration in the complex ω-plane. The denominator has poles at $\omega = 0$ and at the two nonzero roots of the characteristic equation,

$$\mathrm{i}\lambda\omega^3 - m\omega^2 - \mathrm{i}\gamma\omega = 0, \tag{11}$$

which are

$$\omega_{1,2} = -\frac{\mathrm{i}}{2\tau_J} \pm \sqrt{\frac{1}{{\tau_F}^2} - \frac{1}{4\tau_J^2}}\,. \tag{12}$$

Applying the residue theorem, the solution of the third-order linear equation for the Green's function takes the form

$$G(t) = \sum_{j=1}^{3} C_j e^{-i\omega_j t}. \tag{13}$$

The prefactors C_j are determined by matching the continuity conditions of $G(t)$ and its derivatives at $t = 0$. Keeping only the causal ($t > 0$) contributions, we obtain

$$G(t) = \frac{\Theta(t)}{\lambda(\omega_2 - \omega_1)} \sum_{j=1}^{2} (-1)^j \frac{1 - e^{-i\omega_j t}}{\omega_j}. \tag{14}$$

which is the explicit expression for the Green's function for the jcABP dynamics. The nature of the solutions is determined by the real and imaginary parts of ω_j ($j = 1, 2$) given in equation (12). Writing $\omega_j = \omega_R \pm i\omega_I$, the activity-free dynamics is *stable* iff $\omega_I < 0$. When $\tau_F < 2\tau_J$, the square root in equation (12) is real and both frequencies have the same negative imaginary part, $\omega_I = -1/(2\tau_J) < 0$, leading to bounded oscillatory solutions. At the critical value $\tau_F = 2\tau_J$, the two nonzero roots become equal and purely imaginary with $\omega_I = -1/(2\tau_J) < 0$, producing non-oscillatory (purely exponential) decay. For $\tau_F > 2\tau_J$, the square root becomes purely imaginary: writing $\sqrt{1/\tau_F{}^2 - 1/(4\tau_J^2)} = i\beta$ with $0 < \beta < 1/(2\tau_J)$ gives $\omega_I = -1/(2\tau_J) \pm \beta < 0$, so both modes correspond to distinct decaying exponentials. Therefore, when $\lambda, \gamma, m > 0$ (so $\tau_J, \tau_F > 0$), ω_I is never positive and the response remains bounded. However, exponential growth can occur if the parameter signs are not all positive; for example, a system with negative jerk coefficient, negative inertia, or negative friction admits unstable modes. Such cases, while theoretically as well as practically possible in engineered systems [43], will be discussed in detail in section 4.2.

The solution of equation (1) can be written using the convolution:

$$\vec{r}(t) = \int_0^t dt'\, G(t - t') \left(\gamma v_0 \hat{n}(t') + \sqrt{2D\gamma^2}\, \vec{\eta}(t') \right). \tag{15}$$

Taking an ensemble average, we obtain the mean trajectory:

$$\begin{aligned} \langle \vec{r}(t) \rangle &= \gamma v_0 \int_0^t dt'\, G(t - t') \langle \hat{n}(t') \rangle \\ &= \gamma v_0 \int_0^t dt'\, G(t - t') e^{-t'/\tau_P} \begin{pmatrix} \cos(t'/\tau_C) \\ \sin(t'/\tau_C) \end{pmatrix}. \end{aligned} \tag{16}$$

The MSD is then given as

$$\begin{aligned} \mathrm{MSD}(t) &= \langle |\vec{r}(t) - \vec{r}(0)|^2 \rangle \\ &= \int_0^t dt' \int_0^t dt''\, G(t - t')\, G(t - t'') \left[\gamma^2 v_0^2 \langle \hat{n}(t') \cdot \hat{n}(t'') \rangle + 2D\gamma^2 \langle \vec{\eta}(t') \cdot \vec{\eta}(t'') \rangle \right] \\ &= 2\gamma^2 v_0^2 \int_0^t dt' \int_0^{t'} dt''\, \cos[(t' - t'')/\tau_C]\, e^{-(t' - t'')/\tau_P} G(t')\, G(t'') \\ &\quad + 4D\gamma^2 \int_0^t dt'\, G^2(t'). \end{aligned} \tag{17}$$

The first term accounts for activity-induced fluctuations, while the second term arises from translational Brownian noise.

3. Special case of vanishing chirality

Let us first analyze the case where there is no chirality (i.e. $\omega_0 \to 0$ or $\tau_C \to \infty$). This yields the mean displacement

$$\langle \vec{r}(t) \rangle = \gamma v_0 \int_0^t dt'\, G(t - t') \begin{pmatrix} e^{-t'/\tau_P} \\ 0 \end{pmatrix}. \tag{18}$$

This asymmetry in x and y directions arises because the initial orientation is aligned with the x-axis (i.e. $\theta(0) = 0$), and over time, angular diffusion causes the orientation to decorrelate from this direction.

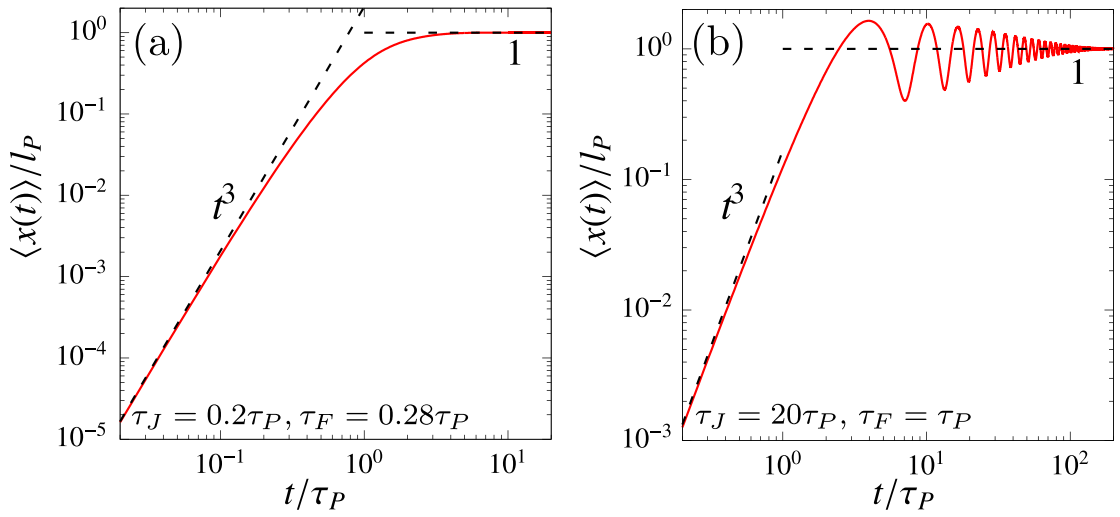

Figure 2. Mean displacement $\langle x(t)\rangle$ in units of the persistence length l_P as a function of the reduced time t/τ_P of a jerky active particle without chirality. The mean displacement grows as t^3 at short times and saturates to l_P for $t \to \infty$, in agreement with the limits of our exact result provided in equation (20). (a) The parameter values used are $\tau_J = 0.2\tau_P$, and $\tau_F = 0.28\tau_P$ corresponding to $\alpha \approx 2.55/\tau_P$. Here, $\tau_P > 2\tau_J$ and there is a smooth exponential relaxation of the mean at large times. (b) The parameter values used are $\tau_J = 20\tau_P$, and $\tau_F = \tau_P$ corresponding to $\alpha \approx 1/\tau_P$. Here, $\tau_P < 2\tau_J$ and we observe oscillations.

However, since there is no chirality and no initial bias in the y-direction, the average motion remains symmetric in y, leading to $\langle y(t)\rangle = 0$. In contrast, the x-component retains a net drift due to the initial alignment, resulting in a nonzero mean: $\langle x(t)\rangle \neq 0$ given as

$$\langle x(t)\rangle = \frac{v_0\tau_P}{{\tau_F}^2\sum_{j=1}^{2}(-1)^j\omega_j}\left[\left(1-\mathrm{e}^{-t/\tau_P}\right)\sum_{j=1}^{2}(-1)^j\frac{1}{\omega_j}+\sum_{j=1}^{2}(-1)^j\frac{\mathrm{e}^{-t/\tau_P}-\mathrm{e}^{-\mathrm{i}\omega_j t}}{\omega_j\left(1-\mathrm{i}\omega_j\tau_P\right)}\right]. \tag{19}$$

Substituting the values of ω_j from equation (12), the above expression can be rewritten in the form

$$\langle x(t)\rangle = v_0\tau_P\left[1-\mathcal{A}_1\mathrm{e}^{-t/\tau_P}++\mathrm{e}^{-t/(2\tau_J)}\left[\mathcal{B}_1\cos(\alpha t)+\mathcal{C}_1\sin(\alpha t)\right]\right], \tag{20}$$

where $v_0\tau_P = l_P$ is the persistence length of an active particle and α is the difference in the eigenfrequencies,

$$\alpha = (\omega_1-\omega_2)/2 = \sqrt{1/{\tau_F}^2 - 1/\left(4\tau_J^2\right)}, \tag{21}$$

the prefactors $\mathcal{A}_1$, $\mathcal{B}_1$, and $\mathcal{C}_1$ are functions of the underlying timescales τ_P, τ_J and τ_F. We have given the explicit expressions of these prefactors in appendix B. Equation (20) has the limiting behaviors

$$\begin{aligned}\langle x(t)\rangle &\overset{t\to 0}{=} \frac{v_0 t^3}{6{\tau_F}^2} - \frac{v_0\left(\frac{1}{\tau_J}+\frac{1}{\tau_P}\right)t^4}{24{\tau_F}^2}+\dots,\\ \langle x(t)\rangle &\overset{t\to\infty}{=} v_0\tau_P = l_P.\end{aligned} \tag{22}$$

Figure 2 shows numerical plots of our analytical expression for the mean displacement given in equation (20). The short-time behavior exhibits a super-ballistic regime with $\langle x(t)\rangle \sim t^3$, while at long time, the mean displacement saturates to the persistence length. Importantly, the qualitative nature of the dynamics is governed by the values of different time scales. If α is imaginary, i.e. $1/{\tau_F}^2 < 1/4\tau_J^2$, the oscillatory terms reduce to purely exponential decay and the relaxation is smooth. If α is real, i.e. $1/{\tau_F}^2 > 1/4\tau_J^2$, the system exhibits oscillations that decay over the timescale $2\tau_J$. The relative magnitudes of τ_P and τ_J determine which decay dominates at long times: for $\tau_P > 2\tau_J$, the jerk-induced oscillations decay faster and the final relaxation is smooth on the timescale τ_P (see figure 2(a)), whereas for $\tau_P < 2\tau_J$, the oscillatory envelope on the timescale $2\tau_J$ dominates the long-time behavior (see figure 2(b)).

For vanishing chirality, the mean squared displacement (MSD) is given as

$$\mathrm{MSD}(t) = \qquad 2\gamma^2 v_0^2\int_0^t \mathrm{d}t'\int_0^{t'}\mathrm{d}t''\,\mathrm{e}^{-\left(t'-t''\right)/\tau_P}G(t')\,G(t'')+\,4D\gamma^2\int_0^t \mathrm{d}t'\,G^2(t'). \tag{23}$$

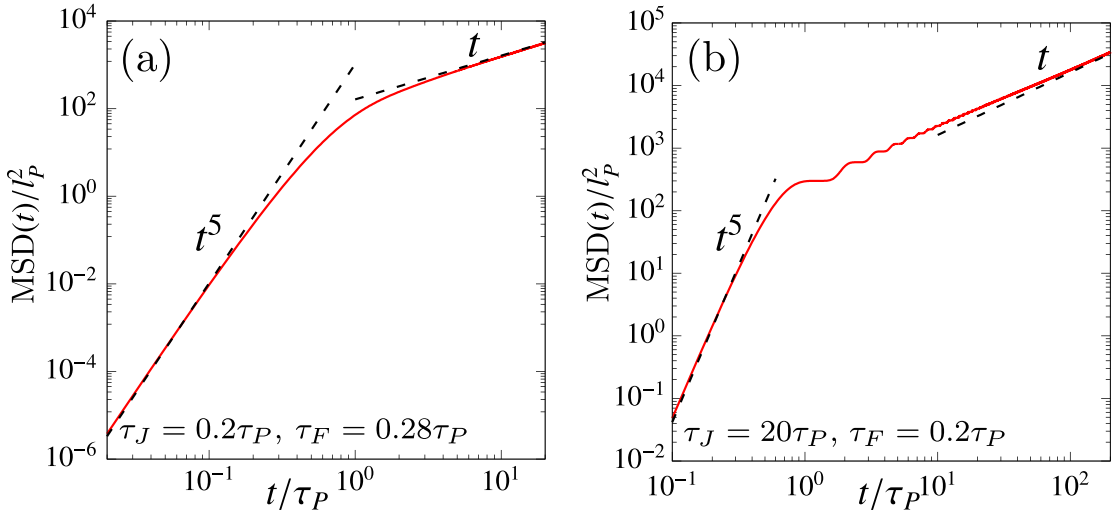

Figure 3. Mean squared displacement in units of l_P^2 as a function of the reduced time t/τ_P of a jerky active particle without chirality given in equation (24). The value $D = 0.5$ is held fixed for both plots. The MSD crosses from MSD$(t) \propto t^5$ at very short times to MSD$(t) \propto t$ at large times. (a) The parameter values used are $\tau_J = 0.2\tau_P$, and $\tau_F = 0.28\tau_P$ corresponding to $\alpha \approx 2.55/\tau_P$. There is a smooth exponential relaxation of the MSD at large times. (b) The parameter values used are $\tau_J = 20\tau_P$, and $\tau_F = 0.2\tau_P$ corresponding to $\alpha \approx 1/\tau_P$. We observe oscillations superimposed on exponential relaxation.

We analytically compute the above expression which has the form:

$$\begin{aligned}\mathrm{MSD}\,(t) = \mathcal{A}_2 t + \mathcal{B}_2 + \mathcal{C}_2 \mathrm{e}^{-t/\tau_P} + \mathcal{D}_2 \mathrm{e}^{-t/\tau_J} + \mathrm{e}^{-t/(2\tau_J)}\left[\mathcal{E}_2 \cos(\alpha t) + \mathcal{F}_2 \sin(\alpha t)\right] \\ + \mathrm{e}^{-t(1/\tau_P + 1/(2\tau_J))}\left[\mathcal{G}_2 \cos(\alpha t) + \mathcal{H}_2 \sin(\alpha t)\right] + \mathrm{e}^{-t/\tau_J}\left[\mathcal{I}_2 \cos(2\alpha t) + \mathcal{J}_2 \sin(2\alpha t)\right].\end{aligned} \tag{24}$$

The prefactors $\{\mathcal{A}_2, \ldots, \mathcal{J}_2\}$ are complicated functions of the underlying timescales, and their explicit forms are provided in appendix B. The parameter α is defined in equation (21). In the asymptotic limits, we obtain

$$\begin{aligned}\mathrm{MSD}\,(t) &\overset{t\to 0}{=} \frac{D t^5}{5{\tau_F}^4} + \left(\frac{v_0^2}{36{\tau_F}^4} - \frac{D}{9\tau_J{\tau_F}^4}\right) t^6 + \ldots\,, \\ \mathrm{MSD}\,(t) &\overset{t\to\infty}{=} \left(4D + 2v_0^2\tau_P\right) t = 4D_{\mathrm{eff}} t,\end{aligned} \tag{25}$$

where $D_{\mathrm{eff}} = D + v_0^2\tau_P/2$ is the *effective diffusion constant* for an active particle [67, 80, 115–117]. Note that in the long-time limit, the MSD is independent of inertia m and jerk λ.

Figure 3 shows numerical plots of our analytical expression for the MSD given in equation (24). The short-time behavior exhibits a super-ballistic regime with MSD$(t) \sim t^5$, while at long times, the MSD grows linearly in t. Similar to the mean displacement, the solution displays visible oscillations superimposed on the exponential relaxation for suitable parameter values. These oscillations reflect an underdamped regime, where the system transiently explores rotational modes before relaxing.

4. Effects of finite chirality

We next analyze the case where the particle has a systematic rotational drift (chirality). Let us first consider the noiseless case where $D_r = 0$.

4.1. Case 1: Zero rotational noise

The mean displacement is given as

$$\langle \vec{r}(t) \rangle = \gamma v_0 \int_0^t \mathrm{d}t' G(t - t') \begin{pmatrix} \cos(t'/\tau_C) \\ \sin(t'/\tau_C) \end{pmatrix}. \tag{26}$$

We compute the analytical expressions for $x(t)$ and $y(t)$ by substituting the expression for the Green's function provided in equation (6). This yields

$$\langle x(t)\rangle = \frac{v_0}{{\tau_F}^2\prod_{j=1}^{2}\left(\omega_j^2-1/\tau_C^2\right)}\left[\frac{\mathrm{i}e^{-\mathrm{i}t\sum_{j=1}^{2}\omega_j}}{\sum_{j=1}^{2}(-1)^j\omega_j}\sum_{j=1}^{2}(-1)^j e^{\mathrm{i}t\omega_j}\left(\omega_j^2-1/\tau_C^2\right)\right. \tag{27}$$
$$\left. -\mathrm{i}\sum_{j=1}^{2}\omega_j\cos(t/\tau_C) - \quad \tau_C\left(\prod_{j=1}^{2}\omega_j+1/\tau_C^2\right)\sin(t/\tau_C)\right],$$
$$\langle y(t)\rangle = \frac{v_0}{{\tau_F}^2\prod_{j=1}^{2}\left(\omega_j^2-1/\tau_C^2\right)}\left[\frac{e^{-\mathrm{i}t\sum_{j=1}^{2}\omega_j}}{\tau_C\sum_{j=1}^{2}(-1)^j\omega_j\prod_{j=1}^{2}\omega_j}\sum_{j=1}^{2}(-1)^j e^{\mathrm{i}t\omega_j}\omega_j\left(\omega_j^2-1/\tau_C^2\right)\right.$$
$$\left. -\tau_C\left(\prod_{j=1}^{2}\omega_j+1/\tau_C^2\right)\cos(t/\tau_C)+\mathrm{i}\sum_{j=1}^{2}\omega_j\sin(t/\tau_C)+\frac{\tau_C\prod_{j=1}^{2}\left(\omega_j^2-1/\tau_C^2\right)}{\prod_{j=1}^{2}\omega_j}\right],$$

where $\sum_{j=1}^{2}\omega_j=-\mathrm{i}/\tau_J$, $\sum_{j=1}^{2}(-1)^j\omega_j=-2\sqrt{1/{\tau_F}^2-1/(4\tau_J^2)}$ and $\prod_{j=1}^{2}\omega_j=-1/{\tau_F}^2$. After substituting the expressions for the eigen-frequencies provided in equation (12), we obtain the compact forms:

$$\langle x(t)\rangle = \mathcal{A}_3\cos(t/\tau_C)+\mathcal{B}_3\sin(t/\tau_C)+e^{-t/(2\tau_J)}\left[\mathcal{C}_3\cos(\alpha t)+\mathcal{D}_3\sin(\alpha t)\right],$$
$$\langle y(t)\rangle = v_0\tau_C-\mathcal{B}_3\cos(t/\tau_C)+\mathcal{A}_3\sin(t/\tau_C)+e^{-t/(2\tau_J)}\left[\mathcal{E}_3\cos(\alpha t)+\mathcal{F}_3\sin(\alpha t)\right]. \tag{28}$$

The prefactors $\{\mathcal{A}_3,\ldots,\mathcal{F}_3\}$ are complicated functions of the underlying timescales, and their explicit forms are provided in appendix B. The above expressions have the limiting behaviors

$$\langle x(t)\rangle \overset{t\to 0}{=} \frac{v_0t^3}{6{\tau_F}^2}-\frac{v_0t^4}{24\tau_J{\tau_F}^2}+\cdots,$$
$$\langle y(t)\rangle \overset{t\to 0}{=} \frac{v_0t^4}{24{\tau_F}^2\tau_C}-\frac{v_0t^5}{120\tau_J{\tau_F}^2\tau_C}+\cdots. \tag{29}$$

After the initial transient regime driven by jerk, inertia and damping, the trajectory converges to a steady circular orbit at large times:

$$\langle x(t)\rangle \overset{t\to\infty}{=} x_c+r\cos(t/\tau_C+\phi),$$
$$\langle y(t)\rangle \overset{t\to\infty}{=} y_c+r\sin(t/\tau_C+\phi), \tag{30}$$

with center

$$(x_c,\ y_c)=(0,v_0\tau_C), \tag{31}$$

radius

$$r=\sqrt{\mathcal{A}_3^2+\mathcal{B}_3^2}=\frac{v_0\tau_C}{\sqrt{{\tau_F}^4/(\tau_J^2\tau_C^2)+\left({\tau_F}^2/\tau_C^2-1\right)^2}}, \tag{32}$$

phase shift

$$\phi=\tan^{-1}(-\mathcal{B}_3/\mathcal{A}_3)=\tan^{-1}\left[\tau_J\left(\tau_C/{\tau_F}^2-1/\tau_C\right)\right], \tag{33}$$

and frequency $\omega_0=1/\tau_C$. We note that the above expressions are non-trivial functions of jerk, friction and chirality. It is well-known that chiral active particles in the absence of rotational noise exhibit circular swimming behavior at large times [93, 103]. The radius of the orbit is determined by the underlying parameters. Equation (32) in the $\lambda\to 0$ limit yields the known expression $r=v_0\gamma/(\omega_0\sqrt{m^2\omega_0^2+\gamma^2})$ for an underdamped ABP with inertia [93] and further in the overdamped limit $m\to 0$, one obtains $r=v_0/\omega_0$. Figure 4 shows the numerical plots of the noise-free analytic expressions for the mean displacements $\langle x(t)\rangle$ and $\langle y(t)\rangle$ in the presence of chirality, given in equation (28). For different parameter choices, all trajectories converge to a circle at long times. However, the initial relaxation is complex and strongly dependent on the parameters.

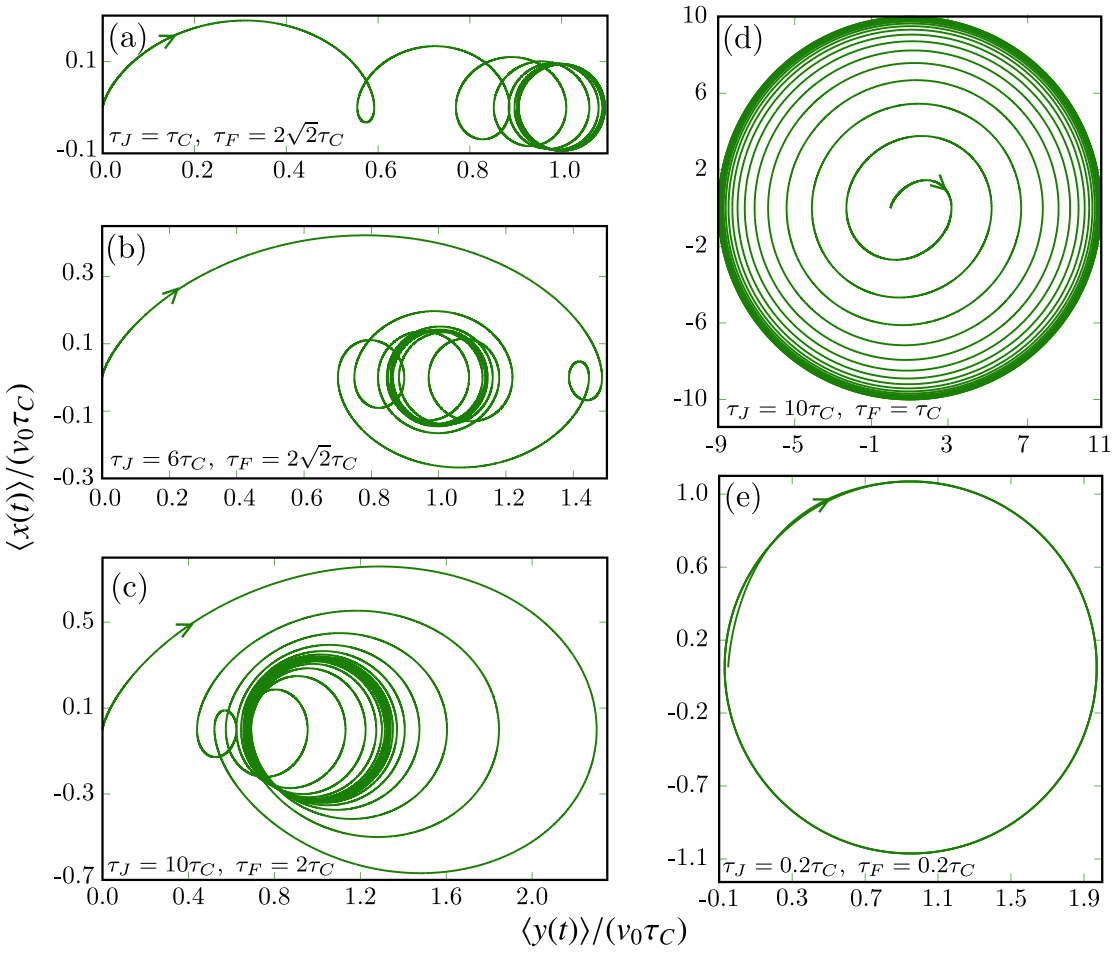

Figure 4. Mean displacement (in units of $v_0\tau_C$) of a jerky active particle with chirality, but in the absence of rotational noise (i.e. $D_r = 0$), provided in equation (28). (a) The timescales are $\tau_J = \tau_C,\ \tau_F = 2\sqrt{2}\tau_C$ corresponding to $\alpha \approx 0.35i/\tau_C$. Note that α is imaginary here. (b) The timescales are $\tau_J = 6\tau_C,\ \tau_F = 2\sqrt{2}\tau_C$ corresponding to $\alpha \approx 0.34/\tau_C$. (c) The timescales are $\tau_J = 10\tau_C,\ \tau_F = 2\tau_C$ corresponding to $\alpha \approx 0.5/\tau_C$. (d) The timescales are $\tau_J = 10\tau_C,\ \tau_F = \tau_C$ corresponding to $\alpha \approx 1/\tau_C$. Note that this is a close to resonance situation where $|\mathrm{Re}[\omega_j]| \approx 1/\tau_C$. (e) The timescales are $\tau_J = 0.2\tau_C,\ \tau_F = 0.2\tau_C$ corresponding to $\alpha \approx 4.3/\tau_C$.

The MSD is given as

$$\mathrm{MSD}\,(t) = 2\gamma^2 v_0^2 \int_0^t \mathrm{d}t' \int_0^{t'} \mathrm{d}t'' \,\cos[(t'-t'')/\tau_C]\, G(t')\, G(t'') + 4D\gamma^2 \int_0^t \mathrm{d}t'\, G^2(t')\,. \tag{34}$$

Since the explicit expression for the MSD is quite large, we list the limiting behaviors

$$\begin{aligned} \mathrm{MSD}\,(t) &\overset{t\to 0}{=} \frac{Dt^5}{5{\tau_F}^4} + \frac{v_0^2 t^6}{36{\tau_F}^4} + \dots\,, \\ \mathrm{MSD}\,(t) &\overset{t\to\infty}{=} 4Dt. \end{aligned} \tag{35}$$

The full dynamical behavior of MSD for two different choices of parameter values is shown in figure 5. Similar to the case of vanishing chirality discussed before, we observe smooth relaxation or oscillatory behavior of MSD depending on the relative magnitude of the timescales.

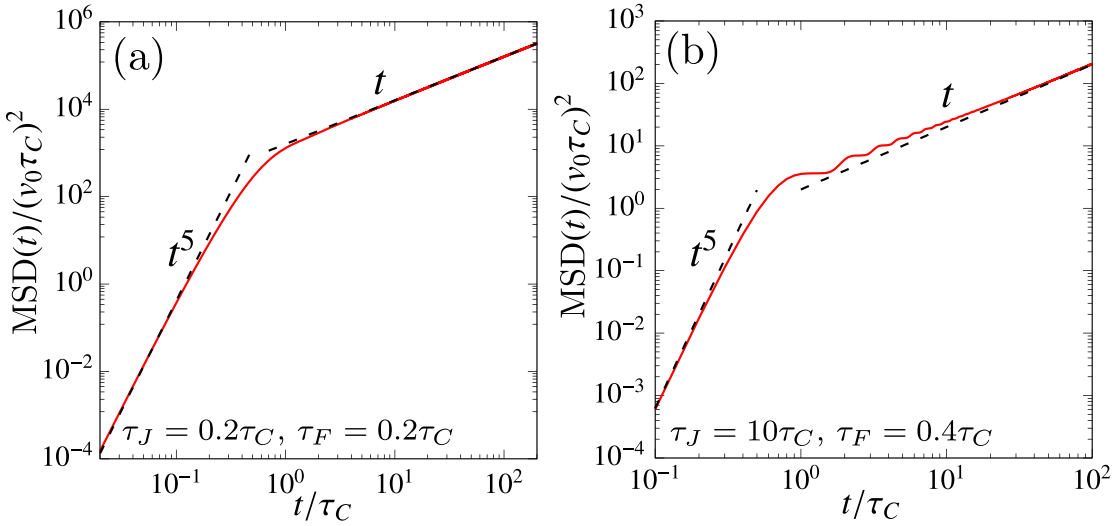

Figure 5. Mean squared displacement (in units of $(v_0\tau_C)^2$) as a function of t/τ_C of a jerky active particle with chirality, but in the absence of rotational noise (i.e. $D_r = 0$), provided in equation (34). The value $D = 0.5$ is kept fixed for both plots. The MSD crosses from $\mathrm{MSD}(t) \propto t^5$ at very short times to $\mathrm{MSD}(t) \propto t$ at large times. (a) The parameter values used are $\tau_J = 0.2\tau_C$, and $\tau_F = 0.2\tau_C$ corresponding to $\alpha \approx 4.3/\tau_C$. (b) The parameter values used are $\tau_J = 10\tau_C$, and $\tau_F = 0.4\tau_C$ corresponding to $\alpha \approx 2.5/\tau_C$.

4.2. Case 1: Non-zero rotational noise

In this section, we consider the effects of finite rotational noise on the dynamics of a jerky chiral active particle. The mean displacement is given by equation (16). After computing the integral, we obtain

$$\begin{aligned}\langle x(t)\rangle &= \frac{v_0}{\tau_P\left(\frac{1}{\tau_P^2}+\frac{1}{\tau_C^2}\right)} + \mathrm{e}^{-t/\tau_P}\left[\mathcal{A}_4\cos(t/\tau_C)+\mathcal{B}_4\sin(t/\tau_C)\right]\\ &\quad + \mathrm{e}^{-t/(2\tau_J)}\left[\mathcal{C}_4\cos(\alpha t)+\mathcal{D}_4\sin(\alpha t)\right],\\ \langle y(t)\rangle &= \frac{v_0}{\tau_P\left(\frac{1}{\tau_P^2}+\frac{1}{\tau_C^2}\right)} + \mathrm{e}^{-t/\tau_P}\left[-\mathcal{B}_4\cos(t/\tau_C)+\mathcal{A}_4\sin(t/\tau_C)\right]\\ &\quad + \mathrm{e}^{-t/(2\tau_J)}\left[\mathcal{E}_4\cos(\alpha t)+\mathcal{F}_4\sin(\alpha t)\right].\end{aligned} \tag{36}$$

The prefactors $\{\mathcal{A}_4,\ldots,\mathcal{F}_4\}$ are complicated functions of the underlying timescales, and their explicit forms are provided in appendix B. The above expressions have the limiting behaviors

$$\begin{aligned}\langle x(t)\rangle &\overset{t\to 0}{=} \frac{v_0 t^3}{6{\tau_F}^2} - \frac{v_0}{24{\tau_F}^2}\left(\frac{1}{\tau_J}+\frac{1}{\tau_P}\right)t^4+\ldots,\\ \langle y(t)\rangle &\overset{t\to 0}{=} \frac{v_0 t^4}{24{\tau_F}^2\tau_C} - \frac{v_0}{60{\tau_F}^2\tau_C}\left(\frac{1}{2\tau_J}+\frac{1}{\tau_P}\right)t^5+\ldots.\end{aligned} \tag{37}$$

At long times, one observes complex trajectory patterns with distortions and oscillations depending on the choice of parameters (see figures 8 and 6). The center of the spiral is given as

$$(x_c^s,\ y_c^s) = \left(\frac{v_0}{\tau_P\left(\frac{1}{\tau_P^2}+\frac{1}{\tau_C^2}\right)}, \frac{v_0}{\tau_C\left(\frac{1}{\tau_P^2}+\frac{1}{\tau_C^2}\right)}\right), \tag{38}$$

and is independent of the values of τ_J and τ_F. Equation (36) can also be rewritten as

$$\begin{aligned}\langle x(t)\rangle &= x_c^s + r_1\mathrm{e}^{-t/\tau_P}\cos(t/\tau_C+\phi_1) + r_2\mathrm{e}^{-t/(2\tau_J)}\cos(\alpha t+\phi_2),\\ \langle y(t)\rangle &= y_c^s + r_1\mathrm{e}^{-t/\tau_P}\sin(t/\tau_C+\phi_1) + r_3\mathrm{e}^{-t/(2\tau_J)}\cos(\alpha t+\phi_3).\end{aligned} \tag{39}$$

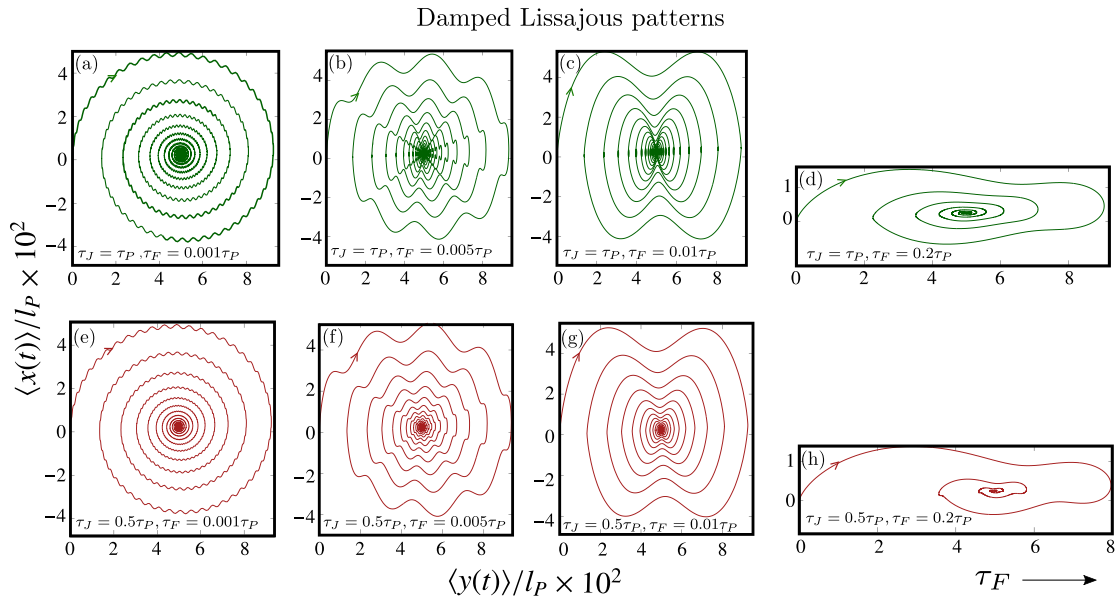

Figure 6. Mean displacement including initial relaxation when $\tau_P \approx 2\tau_J$: mean displacement in units of l_P as a function of the reduced time t/τ_P of a jerky active particle with chirality and rotational noise. The parameter values $\tau_P = 10$, $D = 0.5$, $v_0 = 0.05$ and $\tau_C = 0.05\tau_P$ are fixed for all plots. Plots in the same row correspond to same value of τ_J, but τ_F is varied. (a) $\tau_J = \tau_P, \tau_F = 0.001\tau_P$. (b) $\tau_J = \tau_P, \tau_F = 0.005\tau_P$. (c) $\tau_J = \tau_P, \tau_F = 0.01\tau_P$. (d) $\tau_J = \tau_P, \tau_F = 0.2\tau_P$. (e) $\tau_J = 0.5\tau_P, \tau_F = 0.001\tau_P$. (f) $\tau_J = 0.5\tau_P, \tau_F = 0.005\tau_P$. (g) $\tau_J = 0.5\tau_P, \tau_F = 0.01\tau_P$. (h) $\tau_J = 0.5\tau_P, \tau_F = 0.2\tau_P$. We observe disortions and beats on the spirals.

Equation (39) is a central result of this paper. The constants $r_1 = \sqrt{\mathcal{A}_4^2 + \mathcal{B}_4^2}$, $r_2 = \sqrt{\mathcal{C}_4^2 + \mathcal{D}_4^2}$, $r_3 = \sqrt{\mathcal{E}_4^2 + \mathcal{F}_4^2}$ and the angles $\phi_1 = \tan^{-1}(-\mathcal{B}_4/\mathcal{A}_4)$, $\phi_2 = \tan^{-1}(-\mathcal{D}_4/\mathcal{C}_4)$, $\phi_3 = \tan^{-1}(\mathcal{E}_4/\mathcal{F}_4)$ depend on the values of the underlying parameters. The position vector $\vec{r}(t)$ is given by the superposition of two exponentially decaying oscillatory modes:

$$\langle \vec{r}(t)\rangle = \vec{A}(t) + \vec{B}(t), \tag{40}$$

where $\vec{A}(t)$ traces a circular (logarithmic) spiral, and $\vec{B}(t)$ forms a distorted elliptical spiral (a Lissajous type curve), each characterized by distinct frequencies $1/\tau_C = \omega_0$, α and decay rates τ_P, $2\tau_J$ respectively. Note that $\vec{B}(t)$ is not a circular spiral as $r_2 \neq r_3$ and $\phi_2 \neq \phi_3$. The interference of $\vec{A}(t)$ and $\vec{B}(t)$ generates a complex spiral trajectory. The trajectory becomes distorted and exhibit lobed or beat-like patterns, depending on the interference between the two components (see figure 6). As time progresses, the more slowly decaying mode dominates, and the trajectory asymptotically approaches the corresponding spiral. i.e. if $\tau_P >> 2\tau_J$, $\vec{r}(t) \to \vec{A}(t)$ and if $\tau_P << 2\tau_J$, $\vec{r}(t) \to \vec{B}(t)$ (see figure 7). Note that although logarithmic spirals are self-similar [118], Lissajous curves are not in general self similar. The value of τ_J can be positive or negative depending on the sign of λ and m. For $\tau_J > 0$ (stable case) the trajectory spirals inward (damped spirals) while for $\tau_J < 0$ (unstable case), the trajectories spiral outwards (exploding spirals). The direction of the spirals is set solely by the sign of τ_J (see figure 8).

Figure 9 shows the dependence of the mean trajectories on the characteristic time scales τ_J/τ_C and τ_F/τ_C. Each panel in the figure shows the mean trajectory $\langle y(t)\rangle/l_P \times 10^2$ versus $\langle x(t)\rangle/l_P \times 10^2$ for a specific combination of these parameters. The vertical axis corresponds to increasing τ_J/τ_C, while the horizontal axis corresponds to increasing τ_F/τ_C. As seen from the figure, increasing τ_J/τ_C introduces oscillations that are superimposed on the otherwise spiral trajectories. However, for large τ_F/τ_C, these oscillations are suppressed, and the trajectories become smoother. At the same time, increasing τ_F/τ_C enhances the asymmetry between the x and y components, causing the trajectories to deviate progressively from circular spirals and spread further along the y direction. These observations result from the combined effect of all three time scales τ_J, τ_F, and τ_C. Varying the individual values of these parameters can generate a wide variety of trajectory patterns.

The MSD is given by equation (17). Since this expression is quite large, we list the limiting behaviors

$$\mathrm{MSD}\,(t) \overset{t\to 0}{=} \frac{Dt^5}{5{\tau_F}^4} + \left(\frac{v_0^2}{36{\tau_F}^4} - \frac{D}{9\tau_J{\tau_F}^4}\right) t^6 + \dots, \tag{41}$$

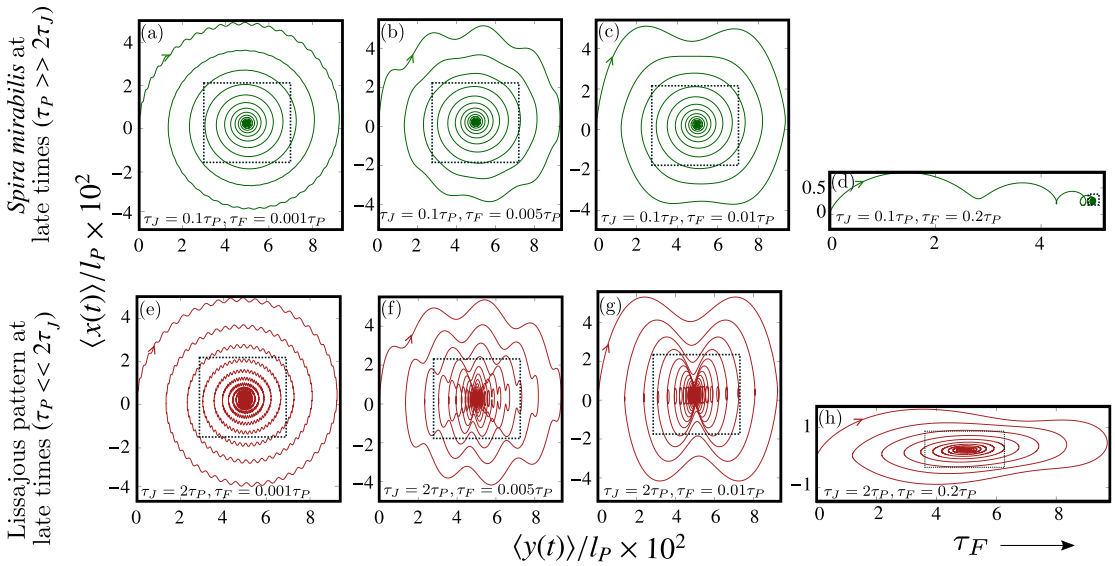

Figure 7. *Spira mirabilis* vs damped Lissajous patterns at large times: mean displacement in units of l_P as a function of the reduced time t/τ_P of a jerky active particle with chirality and rotational noise. The parameter values $\tau_P = 10$, $D = 0.5$, $v_0 = 0.05$ and $\tau_C = 0.05\tau_P$ are fixed for all plots. Plots in the same row correspond to same value of τ_J, but τ_F is varied. Mean displacement including initial relaxation when $\tau_P >> 2\tau_J$: (a) $\tau_J = 0.1\tau_P, \tau_F = 0.001\tau_P$. (b) $\tau_J = 0.1\tau_P, \tau_F = 0.005\tau_P$. (c) $\tau_J = 0.1\tau_P, \tau_F = 0.01\tau_P$. (d) $\tau_J = 0.1\tau_P, \tau_F = 0.2\tau_P$. The trajectories converge to a *spira mirabilis* at large times. Mean displacement including initial relaxation when $\tau_P << 2\tau_J$: (e) $\tau_J = 2\tau_P, \tau_F = 0.001\tau_P$. (f) $\tau_J = 2\tau_P, \tau_F = 0.005\tau_P$. (g) $\tau_J = 2\tau_P, \tau_F = 0.01\tau_P$. (h) $\tau_J = 2\tau_P, \tau_F = 0.2\tau_P$. The trajectories converge to a Lissajous pattern at large times.

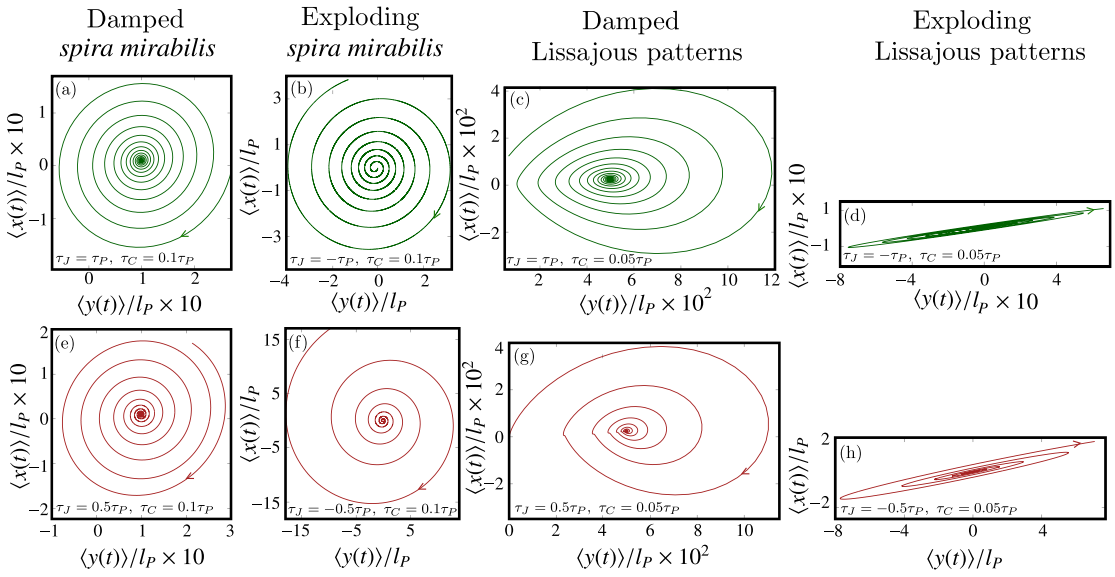

Figure 8. Mean displacement at late times: mean displacement in units of l_P as a function of the reduced time t/τ_P of a jerky active particle with chirality and rotational noise. The parameter values $\tau_P = 10$, $D = 0.5$, $v_0 = 0.05$ and $\tau_F = 0.1\tau_P$ are fixed for all plots. Plots in the same row correspond to same value of $|\tau_J|$, but τ_C is varied. (a) $\tau_J = \tau_P,\ \tau_C = 0.1\tau_P$. (b) $\tau_J = -\tau_P,\ \tau_C = 0.1\tau_P$. (c) $\tau_J = \tau_P,\ \tau_C = 0.05\tau_P$. (d) $\tau_J = -\tau_P,\ \tau_C = 0.05\tau_P$. (e) $\tau_J = 0.5\tau_P,\ \tau_C = 0.1\tau_P$. (f) $\tau_J = -0.5\tau_P,\ \tau_C = 0.1\tau_P$. (g) $\tau_J = 0.5\tau_P,\ \tau_C = 0.05\tau_P$. (h) $\tau_J = -0.5\tau_P,\ \tau_C = 0.05\tau_P$. We observe damped or exploding spirals depending on the sign of τ_J.

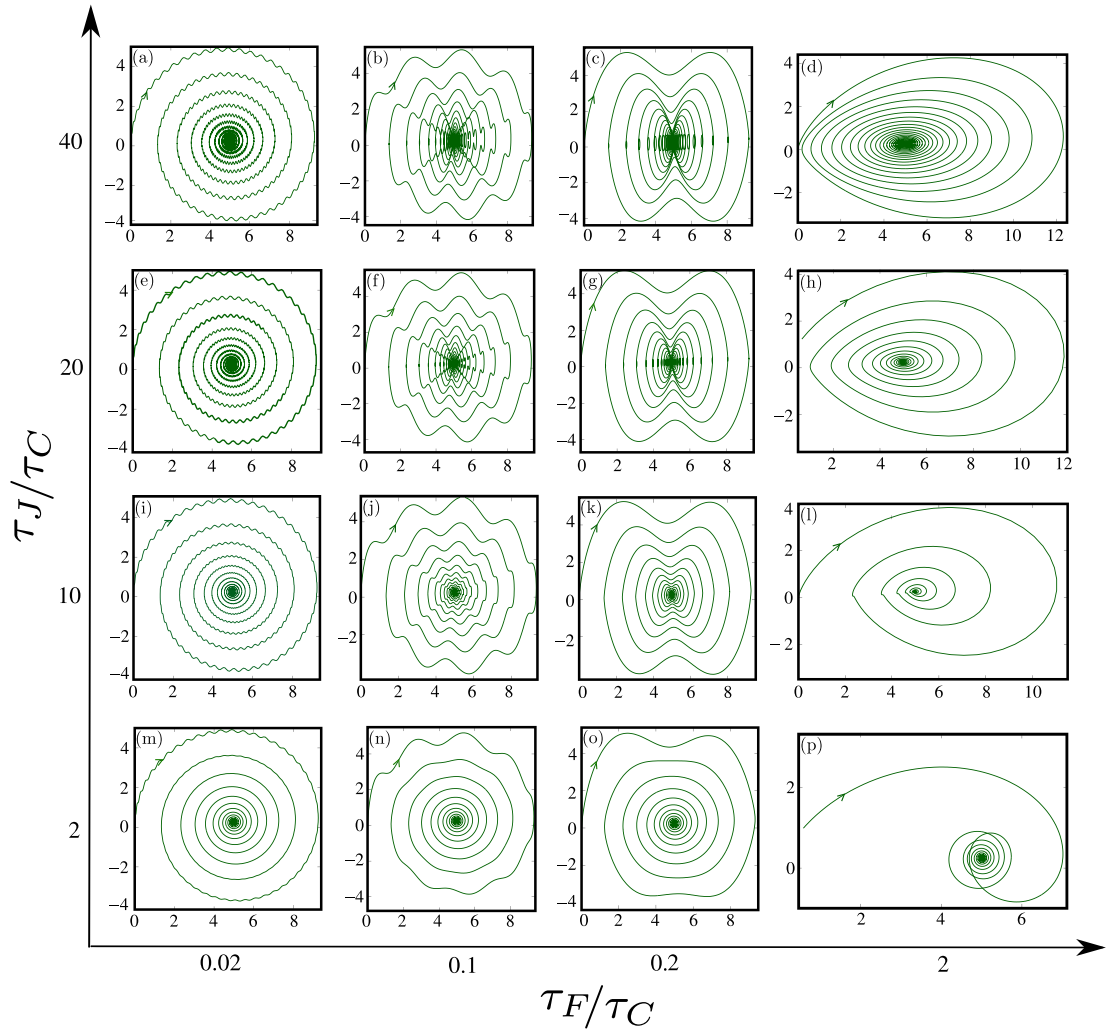

Figure 9. Mean trajectories $\langle y(t)\rangle/l_P \times 10^2$ versus $x(t)/l_P \times 10^2$ for different ratios of τ_J/τ_C (vertical axis) and τ_F/τ_C (horizontal axis). Larger τ_J leads to oscillatory distortions of the otherwise spiral trajectories, while larger τ_F smooths the motion and increases anisotropy between x and y components.

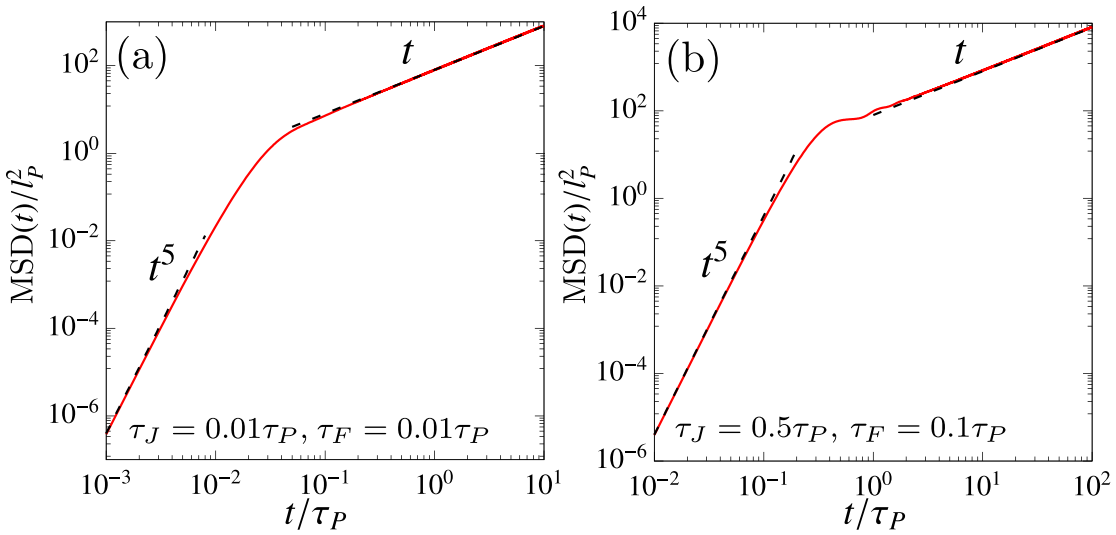

Figure 10. Mean squared displacement of a jerky active particle with both chirality and rotational diffusion given in equation (17). We have set $\tau_P = 10$, $v_0 = 0.05$, and $\tau_C = 0.5$. The MSD crosses from $\mathrm{MSD}(t) \propto t^5$ at very short times to $\mathrm{MSD}(t) \simeq 4D_c t$ at large times. (a) The parameter values used are $\tau_J = 0.01\tau_P$, and $\tau_F = 0.01\tau_P$. (b) The parameter values used are $\tau_J = 0.5\tau_P$, and $\tau_F = 0.1\tau_P$.

and

$$\mathrm{MSD}\,(t) \overset{t\to\infty}{=} \left(4D + \frac{2v_0^2}{\left(\frac{1}{\tau_P} + \frac{\tau_P}{\tau_C^2}\right)}\right) t = 4D_c t, \tag{42}$$

where $D_c = D + \frac{v_0^2}{2\left(1/\tau_P + \tau_P/\tau_C^2\right)}$ is the *effective diffusion constant* for an active particle with chirality [103]. The full dynamical behavior of MSD for two different choices of parameter values is shown in figure 10. Similar to the cases discussed before, we observe smooth relaxation or oscillatory behavior of MSD depending on the relative magnitude of the timescales.

5. Conclusions and discussion

In this work, we introduced a new class of active particles that incorporate both jerk and chirality, namely a jcABP model. Understanding the behavior of a single active particle with jerk provides valuable insight into the roles of memory and delayed response in active systems. Without chirality, jerky active particles exhibit distinct short-time behavior compared to conventional active particles. The mean displacement grows as $\langle x(t)\rangle \sim t^3$ while the MSD follows $\mathrm{MSD}(t) \sim t^5$ for very short times. At intermediate times, the particle experiences transient oscillations or smooth relaxation, a condition captured by the parameter $\alpha = \sqrt{1/{\tau_F}^2 - 1/(4\tau_J^2)}$. If α is imaginary, the relaxation is smooth and if α is real, the system exhibits oscillations that decay over the jerk timescale τ_J. The relative magnitudes of τ_P and τ_J determine which decay dominates at long times: for $\tau_P > 2\tau_J$, the jerk-induced oscillations decay faster and the final relaxation is smooth on the timescale τ_P, whereas for $\tau_P < 2\tau_J$, the oscillations dominate. At long times, these transient effects decay and the particle crosses over to normal active diffusion with an effective diffusion constant [67, 115, 116]. When chirality is included but rotational noise is absent, the mean trajectories eventually settle into circular orbits whose radius and phase depend non-trivially on the interplay of jerk, friction, and chirality. The relaxation toward these orbits is complex and depend on the values of the various underlying time scales.

In the presence of both chirality and rotational noise, the dynamics become even richer. Interestingly, jerk not only modifies the standard circular swimming behavior of chiral active particles but also gives rise to complex spiral trajectories and oscillatory patterns, revealing new dynamical features. The mean trajectory is no longer a simple spiral but rather the superposition of two exponentially decaying oscillatory modes: one associated with the chiral rotation at frequency $1/\tau_C$ and persistence time τ_P, and another with the intrinsic frequency α and decay time $2\tau_J$. The interference of these two modes produces intricate distorted spiral patterns resembling damped or exploding Lissajous curves. Depending on the relative magnitudes of τ_P and τ_J, the particle's trajectory can converge either to a smooth logarithmic spiral or to a modulated Lissajous spiral at long times. The sign of the jerk parameter determines the overall stability: positive τ_J corresponds to inward, damped spirals, while negative τ_J leads to outward, exploding spirals. Despite these transient complexities, the long-time MSD again recovers a linear growth with an effective diffusion coefficient, consistent with known results for chiral active Brownian motion [103].

Looking forward, several promising directions emerge from this work. Future studies could extend the present model to higher spatial dimensions, incorporate higher-order dynamical derivatives, or explore collective phenomena in interacting many-particle systems. For example, models of interacting active particles display rich collective phenomena, including motility-induced phase separation (MIPS), clustering, and flocking [119–123]. At the continuum level, hydrodynamic theories have been developed to describe polar and nematic order in dense active fluids. More recent studies have also investigated activity-induced pattern formation in confined geometries [124, 125], responses to external fields [126, 127], and collective dynamics in chiral systems [128, 129]. Our work can be extended to include memory effects into these broader theoretical frameworks. In the collective regime, the interplay between chirality, jerk, and interactions presents several intriguing open questions. For ordinary circle swimmers, it is now established that chirality generally suppresses conventional MIPS and promotes finite counter-rotating clusters or vortex-like phases, depending on angular velocity [130–134]. Incorporating jerk as an additional degree of freedom may further enrich these behaviors, potentially modifying both the onset and character of phase separation. Extending our single-particle jerky chiral model to many-body systems is therefore a natural and promising direction for future work.

While our present formulation introduces jerk only in the translational dynamics, an intriguing extension is to consider rotational jerk; the time derivative of angular acceleration in the orientational equation of motion. Such a term would naturally arise in systems where the torque acting on a

particle responds with a delay or depends on the time history of angular acceleration, introducing a new intrinsic timescale analogous to τ_J in translation. This would affect the orientational correlations and consequently, the particle trajectories would acquire additional structure. Such an extension would thus provide a unified framework where both translational and angular motion exhibit memory.

Another interesting direction concerns jcABPs in structured environments. Chiral active particles are already known to be exquisitely sensitive to environmental geometry, showing commensuration effects, anomalous diffusion, and chirality-dependent directional locking in periodic lattices [135–137]. Adding jerk into such settings would introduce additional timescales. The interplay between these dynamical timescales and the substrate periodicity could lead to qualitatively new regimes, potentially modifying the rectification behaviors observed in conventional chiral systems. On asymmetric (ratchet-like) substrates, inertial effects are known to produce current reversals [138]. Extending such studies to jerky or higher-order dynamical systems could therefore provide new insight into how memory and geometry together shape active transport. Overall, the jcABP represents a fundamental step toward understanding how higher-order temporal dynamics and circle swimming can reshape motion in active matter. The analytical framework developed here provides exact benchmarks for simulations and experiments, and offers a natural basis for constructing many-body and continuum theories where jerk and chirality together drive new non-equilibrium phenomena.

Data availability statement

All data that support the findings of this study are included within the article (and any supplementary files).

Acknowledgments

S J acknowledges support from the Alexander von Humboldt Foundation through a Humboldt Research Fellowship. H L acknowledges funding of the German Research Foundation (DFG) Project LO 418/29-1.

Appendix A. Orientation correlations

Integrating equation (2) gives the angular displacement:

$$\theta(t) = \omega_0 t + \sqrt{2D_r}\int_0^t \mathrm{d}t'\,\eta_r(t'). \tag{43}$$

Since $\theta(t)$ is a Gaussian process with mean $\langle\theta(t)\rangle = \omega_0 t$ and variance

$$\langle[\theta(t) - \langle\theta(t)\rangle]^2\rangle_c = 2D_r t, \tag{44}$$

we can use the identity for Gaussian averages:

$$\langle \mathrm{e}^{\mathrm{i}\theta(t)}\rangle = \mathrm{e}^{\mathrm{i}\langle\theta(t)\rangle}\mathrm{e}^{-\frac{1}{2}\langle[\theta(t)-\langle\theta(t)\rangle]^2\rangle_c} = \mathrm{e}^{\mathrm{i}\omega_0 t}\mathrm{e}^{-D_r t}. \tag{45}$$

Separating real and imaginary parts gives

$$\langle\cos\theta(t)\rangle = \mathrm{e}^{-D_r t}\cos(\omega_0 t), \tag{46}$$

$$\langle\sin\theta(t)\rangle = \mathrm{e}^{-D_r t}\sin(\omega_0 t). \tag{47}$$

Thus, the average orientation vector is

$$\langle\hat{n}(t)\rangle = \mathrm{e}^{-D_r t}\begin{pmatrix}\cos(\omega_0 t)\\ \sin(\omega_0 t)\end{pmatrix}. \tag{48}$$

To compute the orientation autocorrelation function, we consider

$$\langle\hat{n}(t_1)\cdot\hat{n}(t_2)\rangle = \langle\cos[\theta(t_1) - \theta(t_2)]\rangle. \tag{49}$$

Let $\Delta t = |t_1 - t_2|$. Then,

$$\theta(t_1) - \theta(t_2) = \omega_0\Delta t + \sqrt{2D_r}\int_{t_2}^{t_1}\mathrm{d}t'\,\eta_r(t'), \tag{50}$$

and therefore

$$\langle \cos\left[\theta\left(t_1\right)-\theta\left(t_2\right)\right]\rangle = \langle \cos\left(\omega_0\Delta t+\sqrt{2D_r}\int_{t_2}^{t_1} \mathrm{d}t'\ \eta_r\left(t'\right)\right)\rangle$$
$$= \cos\left(\omega_0\Delta t\right)\ \mathrm{e}^{-D_r\Delta t}. \tag{51}$$

This gives the orientation correlation function given in equation (5).

Appendix B. Expressions for prefactors

$$\mathcal{A}_1 = \frac{\tau_J\tau_P^2}{\tau_J\tau_P^2+{\tau_F}^2\left(\tau_J-\tau_P\right)},$$
$$\mathcal{B}_1 = -\frac{2\tau_J^2\tau_P+{\tau_F}^2\left(\tau_J-\tau_P\right)}{2\alpha\tau_J\left({\tau_F}^2\left(\tau_J-\tau_P\right)+\tau_J\tau_P^2\right)},$$
$$\mathcal{C}_1 = -\frac{{\tau_F}^2\left(\tau_J-\tau_P\right)}{{\tau_F}^2\left(\tau_J-\tau_P\right)+\tau_J\tau_P^2}, \tag{52}$$

$$\mathcal{A}_2 = 4D+2v_0^2\tau_P,$$
$$\mathcal{B}_2 = \frac{2D\left(-3{\tau_F}^2+\tau_J^2\right)}{\tau_J}-\frac{v_0^2\tau_P\left(2\tau_J^2\tau_P^3+3{\tau_F}^4\left(\tau_J+\tau_P\right)-{\tau_F}^2\left(\tau_J^3-4\tau_J\tau_P^2\right)\right)}{\tau_J^2\tau_P^2+{\tau_F}^2\tau_J\left(\tau_J+\tau_P\right)},$$
$$\mathcal{C}_2 = \frac{2v_0^2\tau_J\tau_P^4}{{\tau_F}^2\left(\tau_J-\tau_P\right)+\tau_J\tau_P^2},$$
$$\mathcal{D}_2 = \frac{2\tau_J^3\left(4D\tau_J\tau_P^2+{\tau_F}^2\left(2\tau_J\left(2D+v_0^2\tau_P\right)-\tau_P\left(4D+v_0^2\tau_P\right)\right)\right)}{\left({\tau_F}^2-4\tau_J^2\right)\left({\tau_F}^2\left(\tau_J-\tau_P\right)+\tau_J\tau_P^2\right)},$$
$$\mathcal{E}_2 = \frac{4{\tau_F}^4\left(\tau_J-\tau_P\right)\left(2D+v_0^2\tau_P\right)+2{\tau_F}^2\tau_J\tau_P^2\left(4D+v_0^2\left(\tau_J+\tau_P\right)\right)}{\tau_J\left({\tau_F}^2\left(\tau_J-\tau_P\right)+\tau_J\tau_P^2\right)},$$
$$\mathcal{F}_2 = \frac{4{\tau_F}^5\left(\tau_J-\tau_P\right)\left(2D+v_0^2\tau_P\right)-4\tau_F\tau_J^3\tau_P^2\left(4D+v_0^2\tau_P\right)+2{\tau_F}^3\tau_J\left(-4\tau_J^2\left(2D+v_0^2\tau_P\right)+\tau_P^2\left(4D+v_0^2\tau_P\right)+\tau_J\tau_P\left(8D+5v_0^2\tau_P\right)\right)}{\tau_J\sqrt{-{\tau_F}^2+4\tau_J^2}\left({\tau_F}^2\left(\tau_J-\tau_P\right)+\tau_J\tau_P^2\right)},$$
$$\mathcal{G}_2 = -\frac{2v_0^2{\tau_F}^2\tau_J\tau_P^4\left(\tau_J+\tau_P\right)}{2{\tau_F}^2\tau_J^2\tau_P^2+\tau_J^2\tau_P^4+{\tau_F}^4\left(\tau_J^2-\tau_P^2\right)},$$
$$\mathcal{H}_2 = -\frac{2v_0^2\tau_F\tau_J\tau_P^4\left(-2\tau_J^2\tau_P+{\tau_F}^2\left(\tau_J+\tau_P\right)\right)}{\sqrt{-{\tau_F}^2+4\tau_J^2}\left(2{\tau_F}^2\tau_J^2\tau_P^2+\tau_J^2\tau_P^4+{\tau_F}^4\left(\tau_J^2-\tau_P^2\right)\right)},$$
$$\mathcal{I}_2 = -\frac{{\tau_F}^2\left(v_0^2\left(2\tau_J^4+{\tau_F}^4\left(1-\frac{\tau_J}{\tau_P}\right)+{\tau_F}^2\tau_J^2\left(-4+\frac{3\tau_J}{\tau_P}\right)\right)+2D\left(-{\tau_F}^2+3\tau_J^2\right)\left(\tau_J+\frac{{\tau_F}^2\left(\tau_J-\tau_P\right)}{\tau_P^2}\right)\right)}{\tau_J\left(-{\tau_F}^2+4\tau_J^2\right)\left(\tau_J+\frac{{\tau_F}^2\left(\tau_J-\tau_P\right)}{\tau_P^2}\right)},$$
$$\mathcal{J}_2 = \frac{2D\tau_F\tau_J^3\tau_P^2-{\tau_F}^5\left(\tau_J-\tau_P\right)\left(2D+v_0^2\tau_P\right)+{\tau_F}^3\tau_J\left(-2D\tau_P^2-2\tau_J\tau_P\left(D+v_0^2\tau_P\right)+\tau_J^2\left(2D+v_0^2\tau_P\right)\right)}{\tau_J\sqrt{-{\tau_F}^2+4\tau_J^2}\left({\tau_F}^2\left(\tau_J-\tau_P\right)+\tau_J\tau_P^2\right)}. \tag{53}$$

$$\mathcal{A}_3 = -\frac{v_0{\tau_F}^2\tau_J}{\frac{{\tau_F}^4}{\tau_C^2}+\left(-1+\frac{{\tau_F}^2}{\tau_C^2}\right)^2\tau_J^2},$$
$$\mathcal{B}_3 = \frac{v_0\tau_C^3\left(\tau_C^2-{\tau_F}^2\right)\tau_J^2}{\tau_C^2{\tau_F}^4+\left(\tau_C^2-{\tau_F}^2\right)^2\tau_J^2},$$
$$\mathcal{C}_3 = \frac{v_0{\tau_F}^2\tau_J}{\frac{{\tau_F}^4}{\tau_C^2}+\left(-1+\frac{{\tau_F}^2}{\tau_C^2}\right)^2\tau_J^2},$$
$$\mathcal{D}_3 = \frac{v_0\tau_F\tau_J\left({\tau_F}^2+2\left(-1+\frac{{\tau_F}^2}{\tau_C^2}\right)\tau_J^2\right)}{\sqrt{-{\tau_F}^2+4\tau_J^2}\left(\frac{{\tau_F}^4}{\tau_C^2}+\left(-1+\frac{{\tau_F}^2}{\tau_C^2}\right)^2\tau_J^2\right)},$$
$$\mathcal{E}_3 = \frac{v_0{\tau_F}^2\left({\tau_F}^2+\left(-1+\frac{{\tau_F}^2}{\tau_C^2}\right)\tau_j^2\right)}{\tau_C\left(\frac{{\tau_F}^4}{\tau_C^2}+\left(-1+\frac{{\tau_F}^2}{\tau_C^2}\right)^2\tau_j^2\right)},$$

$$\mathcal{F}_3 = \frac{v_0 {\tau_F}^3 \left({\tau_F}^2 + \left(-3 + \frac{{\tau_F}^2}{\tau_C^2} \right) \tau_j^2 \right)}{\tau_C \sqrt{-{\tau_F}^2 + 4\tau_j^2} \left(\frac{{\tau_F}^4}{\tau_C^2} + \left(-1 + \frac{{\tau_F}^2}{\tau_C^2} \right)^2 \tau_j^2 \right)}, \tag{54}$$

$$\begin{aligned}
\mathcal{A}_4 &= -\frac{v_0 \tau_C^4 {\tau_F}^2 \tau_P^3 \left(\tau_P^2 \left(-3 + \tau_J \tau_P \right) + \tau_C^2 \left(1 - \tau_J \tau_P + {\tau_F}^2 \tau_P^2 \right) \right)}{\left(\tau_C^2 + \tau_P^2 \right) \left(\tau_P^4 + \tau_C^4 \left(1 - \tau_J \tau_P + {\tau_F}^2 \tau_P^2 \right)^2 + \tau_C^2 \tau_P^2 \left(2 - 2\tau_J \tau_P + \left(-2{\tau_F}^2 + \tau_J^2 \right) \tau_P^2 \right) \right)}, \\
\mathcal{B}_4 &= \frac{v_0 \tau_C^3 {\tau_F}^2 \tau_P^4 \left(-\tau_P^2 + \tau_C^2 \left(3 - 2\tau_J \tau_P + {\tau_F}^2 \tau_P^2 \right) \right)}{\left(\tau_C^2 + \tau_P^2 \right) \left(\tau_P^4 + \tau_C^4 \left(1 - \tau_J \tau_P + {\tau_F}^2 \tau_P^2 \right)^2 + \tau_C^2 \tau_P^2 \left(2 - 2\tau_J \tau_P + \left(-2{\tau_F}^2 + \tau_J^2 \right) \tau_P^2 \right) \right)}, \\
\mathcal{C}_4 &= \frac{v_0 \tau_C^2 \tau_P \left(-\tau_P^2 - \tau_C^2 \left(-1 + \tau_J \tau_P \right) \left(-1 + \tau_P \left(\tau_J - {\tau_F}^2 \tau_P \right) \right) \right)}{\tau_P^4 + \tau_C^4 \left(1 - \tau_J \tau_P + {\tau_F}^2 \tau_P^2 \right)^2 + \tau_C^2 \tau_P^2 \left(2 - 2\tau_J \tau_P + \left(-2{\tau_F}^2 + \tau_J^2 \right) \tau_P^2 \right)}, \\
\mathcal{D}_4 &= \frac{v_0 \tau_C^2 \tau_P \left(\tau_P^2 \left(-\tau_J + 2{\tau_F}^2 \tau_P \right) - \tau_C^2 \left(-\tau_J + \left(-2{\tau_F}^2 + \tau_J^2 \right) \tau_P \right) \left(-1 + \tau_P \left(\tau_J - {\tau_F}^2 \tau_P \right) \right) \right)}{\sqrt{4{\tau_F}^2 - \tau_J^2} \left(\tau_P^4 + \tau_C^4 \left(1 - \tau_J \tau_P + {\tau_F}^2 \tau_P^2 \right)^2 + \tau_C^2 \tau_P^2 \left(2 - 2\tau_J \tau_P + \left(-2{\tau_F}^2 + \tau_J^2 \right) \tau_P^2 \right) \right)}, \\
\mathcal{E}_4 &= -\frac{v_0 \tau_C \tau_P^2 \left(\tau_P^2 + \tau_C^2 \left(1 - 2\tau_J \tau_P + \left(-{\tau_F}^2 + \tau_J^2 \right) \tau_P^2 \right) \right)}{\tau_P^4 + \tau_C^4 \left(1 - \tau_J \tau_P + {\tau_F}^2 \tau_P^2 \right)^2 + \tau_C^2 \tau_P^2 \left(2 - 2\tau_J \tau_P + \left(-2{\tau_F}^2 + \tau_J^2 \right) \tau_P^2 \right)}, \\
\mathcal{F}_4 &= \frac{v_0 \tau_C \tau_P^2 \left(-\tau_J \tau_P^2 - \tau_C^2 \left(4{\tau_F}^2 \tau_P + \tau_J \left(1 - 2\tau_J \tau_P + \left(-3{\tau_F}^2 + \tau_J^2 \right) \tau_P^2 \right) \right) \right)}{\sqrt{4{\tau_F}^2 - \tau_J^2} \left(\tau_P^4 + \tau_C^4 \left(1 - \tau_J \tau_P + {\tau_F}^2 \tau_P^2 \right)^2 + \tau_C^2 \tau_P^2 \left(2 - 2\tau_J \tau_P + \left(-2{\tau_F}^2 + \tau_J^2 \right) \tau_P^2 \right) \right)}.
\end{aligned} \tag{55}$$

ORCID iDs

Stephy Jose 0000-0002-5089-9873
Hartmut Löwen 0000-0001-5376-8062

References

[1] Transon A 1845 *J. Math. Pures Appl.* **10** 320–6 (available at: https://www.numdam.org/item/JMPA_1845_1_10__320_0/)
[2] Meyer zur Capellen W 1959 *Ing.-Arch.* **27** 53–65
[3] Schot S H 1978 *Am. J. Phys.* **46** 1090–4
[4] Linz S J 1997 *Am. J. Phys.* **65** 523–6
[5] Eichhorn R, Linz S J and Hänggi P 1998 *Phys. Rev. E* **58** 7151
[6] Eichhorn R, Linz S J and Hänggi P 2002 *Chaos Solitons Fractals* **13** 1–15
[7] Klages R, Lucero-Azuara N, Kumar V, Gentili A, Torres P, Eizaguirre C, Volpe G and Palyulin V 2025 Modelling the movements of organisms: from cell migration to bumblebee flights to foraging sea turtles *The Mathematics of Movement: an Interdisciplinary Approach to Mutual Challenges in Animal Ecology and Cell Biology* (Springer)
[8] Liu F, Cheng R, Zheng P and Ge H 2016 *Nonlinear Dyn.* **83** 793–800
[9] Jackson J D 2021 *Classical Electrodynamics* (Wiley)
[10] Popławski N J 2006 *Phys. Lett. B* **640** 135–7
[11] Mori H 1965 *Prog. Theor. Phys.* **33** 423–55
[12] Zwanzig R 1961 *Phys. Rev.* **124** 983–92
[13] Mori H 1965 *Prog. Theor. Phys.* **34** 399–416
[14] Zwanzig R and Bixon M 1970 *Phys. Rev. A* **2** 2005–12
[15] Español P and Zúñiga I 1993 *J. Chem. Phys.* **98** 574–80
[16] Bocquet L, Piasecki J and Hansen J P 1994 *J. Stat. Phys.* **76** 505–26
[17] Mason T G and Weitz D A 1995 *Phys. Rev. Lett.* **74** 1250–3
[18] Nakajima S 1958 *Prog. Theor. Phys.* **20** 948–59
[19] Leung A Y T, Yang H and Zhu P 2014 *Int. J. Bifurcation Chaos* **24** 1450028
[20] Keim N C, Paulsen J D, Zeravcic Z, Sastry S and Nagel S R 2019 *Rev. Mod. Phys.* **91** 035002
[21] Kowalik B, Daldrop J O, Kappler J, Schulz J C F, Schlaich A and Netz R R 2019 *Phys. Rev. E* **100** 012126
[22] Straube A V, Kowalik B G, Netz R R and Höfling F 2020 *Commun. Phys.* **3** 126
[23] Goychuk I 2022 *Proc. Natl Acad. Sci.* **119** e2205637119
[24] Scalfi L, Vitali D, Kiefer H and Netz R R 2023 *J. Chem. Phys.* **158** 191101
[25] Mitterwallner B G, Schreiber C, Daldrop J O, Rädler J O and Netz R R 2020 *Phys. Rev. E* **101** 32408
[26] Klimek A and Netz R R 2022 *Europhys. Lett.* **139** 32003
[27] Klimek A, Mondal D, Block S, Sharma P and Netz R R 2024 *Biophys. J.* **123** 1173–83
[28] Dalton B A, Klimek A, Kiefer H, Brünig F N, Colinet H, Tepper L, Abbasi A and Netz R R 2025 *Annu. Rev. Phys. Chem.* **76** 431–54
[29] Milster S, Koch F, Widder C, Schilling T and Dzubiella J 2024 *J. Chem. Phys.* **160** 094901
[30] Wiśniewski M, Łuczka J and Spiechowicz J 2024 *Phys. Rev. E* **109** 044116
[31] Umut O and Yaşar S 2013 *Int. J. Mod. Nonlinear Theory Appl.* **2** 60–68
[32] Rajagopal K, Takougang Kingni S, Fautso Kuiate G, Kamdoum Tamba V and Pham V T 2018 *Adv. Math. Phys.* **2018** 7273531
[33] Wu B, Lim C and Sun W 2006 *Phys. Lett. A* **354** 95–100
[34] Gottlieb H 1998 *Am. J. Phys.* **66** 903–6
[35] Gottlieb H 2004 *J. Sound Vib.* **271** 671–83
[36] Gottlieb H 2006 *J. Sound Vib.* **297** 243–50

[37] Gomez-Solano J R and Bechinger C 2015 *New J. Phys.* **17** 103032
[38] Puertas A M and Voigtmann T 2014 *J. Phys.: Condens. Matter* **26** 243101
[39] Narinder N, Bechinger C and Gomez-Solano J R 2018 *Phys. Rev. Lett.* **121** 078003
[40] Treffenstädt L L and Schmidt M 2020 *Soft Matter* **16** 11006–14
[41] Dalton B A, Kiefer H and Netz R R 2024 *Nat. Commun.* **15** 48016
[42] Sprenger A R, Bair C and Löwen H 2022 *Phys. Rev. E* **105** 044610
[43] Löwen H 2025 arXiv:2507.08910
[44] Bechhoefer J 2005 *Rev. Mod. Phys.* **77** 783–836
[45] Van Heerden B, Vickers N A, Krüger T P and Andersson S B 2022 *Small* **18** 2107024
[46] Saha D, Tarama S, Löwen H and Egelhaaf S U 2024 *Soft Matter* **20** 8112–24
[47] Holubec V, Ryabov A, Loos S A and Kroy K 2022 *New J. Phys.* **24** 023021
[48] Kopp R A and Klapp S H 2023 *Europhys. Lett.* **143** 17002
[49] Newton I 1833 *Philosophiae Naturalis Principia Mathematica* vol 1 (G. Brookman)
[50] Loos S A and Godec A 2025 *Phys. A: Math. Theor.* **58** 220301
[51] Paulsen J D and Keim N C 2019 *Proc. R. Soc. A* **475** 20180874
[52] Zhao X, Hartich D and Godec A 2024 *Phys. Rev. Lett.* **132** 147101
[53] Dieball C, Krapf D, Weiss M and Godec A 2022 *New J. Phys.* **24** 023004
[54] Yulmetyev R, Hänggi P and Gafarov F 2000 *Phys. Rev. E* **62** 6178
[55] Kim H J 2014 *Phys. Rev. E* **90** 012103
[56] Stanislavsky A, Weron K and Weron A 2015 *Commun. Nonlinear Sci. Numer. Simul.* **24** 117–26
[57] Korsakas S, Bučinskas J and Abramavicius D 2020 *J. Chem. Phys.* **152** 244114
[58] Bhattacharyya S, Sayer T and Montoya-Castillo A 2025 *Proc. Natl Acad. Sci.* **122** e2424582122
[59] Marchetti M C, Joanny J F, Ramaswamy S, Liverpool T B, Prost J, Rao M and Simha R A 2013 *Rev. Mod. Phys.* **85** 1143–89
[60] Ramaswamy S 2010 *Annu. Rev. Condens. Matter Phys.* **1** 323–45
[61] Bechinger C, Di Leonardo R, Löwen H, Reichhardt C and Volpe G 2016 *Rev. Mod. Phys.* **88** 045006
[62] Gompper G *et al* 2020 *J. Phys.: Condens. Matter* **32** 193001
[63] Berg H C 2004 *E. Coli in Motion* (Springer)
[64] Tailleur J and Cates M E 2008 *Phys. Rev. Lett.* **100** 218103
[65] Ebbens S J and Howse J R 2010 *Soft Matter* **6** 726–38
[66] Golestanian R, Liverpool T B and Ajdari A 2005 *Phys. Rev. Lett.* **94** 220801
[67] Howse J R, Jones R A L, Ryan A J, Gough T, Vafabakhsh R and Golestanian R 2007 *Phys. Rev. Lett.* **99** 048102
[68] Kudrolli A, Lumay G, Volfson D and Tsimring L S 2008 *Phys. Rev. Lett.* **100** 058001
[69] Deseigne J, Dauchot O and Chaté H 2010 *Phys. Rev. Lett.* **105** 098001
[70] Uhlenbeck G E and Ornstein L S 1930 *Phys. Rev.* **36** 823–41
[71] Szamel G 2014 *Phys. Rev. E* **90** 012111
[72] Bonilla L L 2019 *Phys. Rev. E* **100** 022601
[73] Martin D, O'Byrne J, Cates M E, Fodor E, Nardini C, Tailleur J and van Wijland F 2021 *Phys. Rev. E* **103** 032607
[74] Dabelow L and Eichhorn R 2021 *Front. Phys.* **8** 582992
[75] Wittmann R, Brader J M, Sharma A and Marconi U M B 2018 *Phys. Rev. E* **97** 012601
[76] Fritz J H and Seifert U 2023 *J. Stat. Mech.* 093204
[77] Gupta D, Klapp S and Sivak D 2023 *Phys. Rev. E* **108** 024117
[78] Crisanti A and Paoluzzi M 2023 *Phys. Rev. E* **107** 034110
[79] Fily Y and Marchetti M C 2012 *Phys. Rev. Lett.* **108** 235702
[80] Lindner B and Nicola E 2008 *Eur. Phys. J. Spec. Top.* **157** 43–52
[81] Basu U, Majumdar S N, Rosso A and Schehr G 2018 *Phys. Rev. E* **98** 062121
[82] Romanczuk P and Erdmann U 2010 *Eur. Phys. J. Spec. Top.* **187** 127–34
[83] Romanczuk P, BLär M, Ebeling W, Lindner B and Schimansky-Geier L 2012 *Eur. Phys. J. Spec. Top.* **202** 1–162
[84] Cates M E and Tailleur J 2013 *Europhys. Lett.* **101** 20010
[85] Merrigan C, Ramola K, Chatterjee R, Segall N, Shokef Y and Chakraborty B 2020 *Phys. Rev. Res.* **2** 013260
[86] Lee C F 2013 *New J. Phys.* **15** 055007
[87] Jose S, Dandekar R and Ramola K 2023 *J. Stat. Mech.* 083208
[88] Scholz C, Jahanshahi S, Ldov A and Löwen H 2018 *Nat. Commun.* **9** 5156
[89] Sprenger A R, Scholz C, Ldov A, Wittkowski R and Löwen H 2023 *Commun. Phys.* **6** 301
[90] Caprini L, Puglisi A and Marini Bettolo Marconi U 2021 *Phys. Rev. Res.* **3** 013197
[91] Caprini L, Gupta R K and Löwen H 2022 *Phys. Chem. Chem. Phys.* **24** 24910–6
[92] Sprenger A R, Caprini L and Löwen H 2023 *J. Phys.: Condens. Matter* **35** 254001
[93] Sprenger A R, Jahanshahi S, Ivlev A V and Löwen H 2021 *Phys. Rev. E* **103** 042601
[94] Löwen H 2020 *J. Chem. Phys.* **152** 040901
[95] Gutierrez-Martinez L L and Sandoval M 2020 *J. Chem. Phys.* **153** 044906
[96] Nguyen G P, Wittmann R and Löwen H 2021 *J. Phys.: Condens. Matter* **34** 035101
[97] Montana F, Camporeale C, Porporato A and Rondoni L 2023 *Phys. Rev. E* **107** 054607
[98] Caprini L and Marini Bettolo Marconi U 2021 *J. Chem. Phys.* **154** 024902
[99] Caprini L and Marconi U M B 2021 *Soft Matter* **17** 4109–21
[100] Marconi U M B, Caprini L and Puglisi A 2021 *New J. Phys.* **23** 103023
[101] Hecht L, Caprini L, Löwen H and Liebchen B 2024 *J. Chem. Phys.* **161** 224904
[102] Caprini L, Marini Bettolo Marconi U and Puglisi A 2023 *J. Chem. Phys.* **159** 041102
[103] van Teeffelen S and Löwen H 2008 *Phys. Rev. E* **78** 020101
[104] Nosenko V, Luoni F, Kaouk A, Rubin-Zuzic M and Thomas H 2020 *Phys. Rev. Res.* **2** 033226
[105] Zhang B, Sokolov A and Snezhko A 2020 *Nat. Commun.* **11** 4401
[106] Baconnier P, Dauchot O, Démery V, Düring G, Henkes S, Huepe C and Shee A 2025 *Rev. Mod. Phys.* **97** 015007
[107] Bayati P and Nourhani A 2022 *Phys. Rev. E* **105** 024606
[108] Pattanayak A, Shee A, Chaudhuri D and Chaudhuri A 2024 *New J. Phys.* **26** 083024

[109] Kümmel F, ten Hagen B, Wittkowski R, Buttinoni I, Eichhorn R, Volpe G, Löwen H and Bechinger C 2013 *Phys. Rev. Lett.* **110** 198302
[110] Jahanshahi S, Löwen H and ten Hagen B 2017 *Phys. Rev. E* **95** 022606
[111] Kurzthaler C and Franosch T 2017 *Soft Matter* **13** 6396–406
[112] Van Roon D M, Volpe G, da Gama M M T and Araújo N A 2022 *Soft Matter* **18** 6899–906
[113] Van Roon D M, Volpe G, Da Gama M M T and Araújo N A 2025 *Phys. Rev. E* **111** 045405
[114] Te Vrugt M, Jeggle J and Wittkowski R 2021 *New J. Phys.* **23** 063023
[115] Solon A P, Cates M E and Tailleur J 2015 *Eur. Phys. J. Spec. Top.* **224** 1231–62
[116] Aragones J L, Yazdi S and Alexander-Katz A 2018 *Phys. Rev. Fluids* **3** 083301
[117] Jose S 2022 *J. Stat. Mech.* 113208
[118] Babel S, Ten Hagen B and Löwen H 2014 *J. Stat. Mech.* 02011
[119] Cates M E and Tailleur J 2015 *Annu. Rev. Condens. Matter Phys.* **6** 219–44
[120] Buttinoni I, Bialké J, Kümmel F, Löwen H, Bechinger C and Speck T 2013 *Phys. Rev. Lett.* **110** 238301
[121] Redner G S, Hagan M F and Baskaran A 2013 *Biophys. J.* **104** 640a
[122] Vicsek T, Czirók A, Ben-Jacob E, Cohen I and Shochet O 1995 *Phys. Rev. Lett.* **75** 1226
[123] Toner J and Tu Y 1995 *Phys. Rev. Lett.* **75** 4326
[124] Wioland H, Woodhouse F G, Dunkel J, Kessler J O and Goldstein R E 2013 *Phys. Rev. Lett.* **110** 268102
[125] Xu H, Nejad M R, Yeomans J M and Wu Y 2023 *Proc. Natl Acad. Sci.* **120** e2219708120
[126] Shaik V A, Peng Z, Brady J F and Elfring G J 2023 *Soft Matter* **19** 1384–92
[127] Bickmann J, Bröker S, Te Vrugt M and Wittkowski R 2023 *Phys. Rev. E* **108** 044601
[128] Lei T, Zhao C, Yan R and Zhao N 2023 *Soft Matter* **19** 1312–29
[129] Kushwaha D and Mishra S 2025 *Physica A* **677** 130897
[130] Liebchen B and Levis D 2022 *Europhys. Lett.* **139** 67001
[131] Liao G J and Klapp S H 2018 *Soft Matter* **14** 7873–82
[132] Ma Z and Ni R 2022 *J. Chem. Phys.* **156** 021102
[133] Bickmann J, Bröker S, Jeggle J and Wittkowski R 2022 *J. Chem. Phys.* **156** 194904
[134] Sesé-Sansa E, Levis D and Pagonabarraga I 2022 *J. Chem. Phys.* **157** 224905
[135] Chan C W, Wu D, Qiao K, Fong K L, Yang Z, Han Y and Zhang R 2024 *Nat. Commun.* **15** 1406
[136] Nourhani A and Lammert P E 2016 *Phys. Rev. Lett.* **116** 178302
[137] Reichhardt C and Reichhardt C J 2003 *Phys. Rev. E* **68** 046102
[138] Reichhardt C O and Reichhardt C 2017 *Annu. Rev. Condens. Matter Phys.* **8** 51–75